



UNIVERSITY OF LEEDS

This is a repository copy of *Employing non-contact sensing techniques for improving efficiency and automation in numerical modelling of existing masonry structures: A critical literature review*.

White Rose Research Online URL for this paper:  
<https://eprints.whiterose.ac.uk/173717/>

Version: Accepted Version

---

**Article:**

Kassotakis, N and Sarhosis, V [orcid.org/0000-0002-8604-8659](https://orcid.org/0000-0002-8604-8659) (2021) Employing non-contact sensing techniques for improving efficiency and automation in numerical modelling of existing masonry structures: A critical literature review. *Structures*, 32. pp. 1777-1797. ISSN 2352-0124

<https://doi.org/10.1016/j.istruc.2021.03.111>

---

© 2021 Institution of Structural Engineers. This manuscript version is made available under the CC-BY-NC-ND 4.0 license <http://creativecommons.org/licenses/by-nc-nd/4.0/>.

**Reuse**

This article is distributed under the terms of the Creative Commons Attribution-NonCommercial-NoDerivs (CC BY-NC-ND) licence. This licence only allows you to download this work and share it with others as long as you credit the authors, but you can't change the article in any way or use it commercially. More information and the full terms of the licence here: <https://creativecommons.org/licenses/>

**Takedown**

If you consider content in White Rose Research Online to be in breach of UK law, please notify us by emailing [eprints@whiterose.ac.uk](mailto:eprints@whiterose.ac.uk) including the URL of the record and the reason for the withdrawal request.



[eprints@whiterose.ac.uk](mailto:eprints@whiterose.ac.uk)  
<https://eprints.whiterose.ac.uk/>

1 **Employing non-contact sensing techniques for improving efficiency and automation in**  
2 **numerical modelling of existing masonry structures: A critical literature review**

3 Nicko Kassotakis<sup>1</sup>, Vasilis Sarhosis<sup>2</sup>

4 <sup>1</sup>School of Engineering, Newcastle University, Newcastle Upon Tyne, UK

5 <sup>2</sup>School of Civil Engineering, University of Leeds, LS2 9JT, UK  
6

7 **Abstract**

8 This paper presents approaches for the employment of non-contact sensing to enhance both the  
9 efficiency and reliability of numerical modelling of historic masonry. It commences with a thorough  
10 review of the high-level numerical modelling approaches of historic masonry. Following, the accuracy  
11 and cost-effectivity of available non-contact sensing techniques are reviewed for surveying masonry  
12 structures. These are: a) the total station; b) the laser tracker; c) Structure-from-Motion (SfM)  
13 photogrammetry; and d) terrestrial laser scanning (TLS). Then, strategies of automatically developing  
14 geometric models (i.e., numerical models before structural analysis) from geospatial data are reviewed,  
15 considering their potential for automation and usage. These were based on the employment of: a) point  
16 clouds; b) meshes; c) non-uniform rational basis splines (NURBSs); d) building information models  
17 (BIMs); e) orthoimages; and f) discrete points. Primarily, the review found that high-level numerical  
18 modelling approaches such as the continuum and block-based models are highly effective, but  
19 necessitate accurate geometric data for reliable results. To bridge this gap, the potential of emerging  
20 technologies such as SfM photogrammetry was found to significantly improve the efficiency and  
21 robustness of high-level structural analysis, through providing geometric data accurately and with a low  
22 cost. Moreover, the cloud-based (i.e., with a point cloud) and image-based (i.e., with an orthoimage)  
23 approaches of converting geospatial data into numerical models were also found the most effective, for  
24 continuum and block-based modelling respectively. This contribution demonstrates the potential to  
25 employ novel digital technologies such as non-contact sensing techniques to improve the efficiency and  
26 robustness of high-level numerical modelling approaches.

27 **Keywords:** masonry, numerical modelling, non-contact sensing techniques, SfM photogrammetry,  
28 BIM, terrestrial laser scanning, laser tracker

29  
30  
31  
32  
33  
34  
35  
36 Corresponding author: Dr Vasilis Sarhosis, University of Leeds, email: [v.sarhosis@leeds.ac.uk](mailto:v.sarhosis@leeds.ac.uk)

## 37 1 Introduction

38 Historic masonry structures, such as retaining walls, domestic property, bridges, viaducts, tunnels etc  
39 form a significant part of our building stock. Most of our masonry stock is ageing, often is well beyond  
40 100 years old, and showing significant signs of deterioration and distress. Weathering, changing loading  
41 demands, vibrations due to earthquakes and anthropogenic events, plus factors such as increased  
42 frequency of flood events due to climate change have introduced extreme uncertainty in the long-term  
43 performance of such assets. Also, much of our masonry structures have significant heritage and cultural  
44 value (e.g., the Grade II-listed Hungerford Canal Bridge, in Berkshire, England (Garrity, 2013)) and  
45 according to UN Sustainable Development Goal 11 (United Nations, 2016), efforts should be placed on  
46 “retain and repair”, rather than “demolish and replace”. Failure of such structures could lead to direct  
47 and indirect costs to the economy and society. Therefore, there is an urgent need to better understand  
48 the in-service performance of our ageing historic masonry structures and to provide detailed and  
49 accurate data that will better inform maintenance programmes and asset management decisions.

50 However, assessing the structural performance of old and deteriorated historic masonry structures is a  
51 complex task. Previous research has clearly demonstrated that the assessment methods currently used  
52 by the industry are antiquated and/or over-simplistic. For example, for the assessment of masonry arch  
53 bridges, the Military Engineering Experimental Establishment (MEXE) method of assessment is still in  
54 use (Highway Agency, 2001). This method dates back to the 1940s, has a very limited predictive  
55 capability, and offers little scope for future enhancement. Also, although the primary focus of past  
56 research has been into the prediction of structural failure of ageing historic masonry structures,  
57 prediction of the service load above which incremental damage occurs is now a key priority for owners.  
58 Over the last three decades, significant efforts have been devoted to the development of numerical  
59 models to represent the complex and non-linear behaviour of masonry structures subjected to external  
60 loads. Such models range from considering masonry as a continuum (macro-models) to the more  
61 detailed ones that consider masonry as an assemblage of units and mortar joints (block-based models).  
62 However, a vital aspect when modelling masonry structures is the accuracy in which the geometry and  
63 material performance characteristics of the masonry constituents (i.e. masonry units, mortar joints) are  
64 transferred in the numerical model. Geometric model development (or otherwise termed solid model  
65 development), is the procedure of developing the geometry of the structure in an appropriately digital  
66 format so that it can be inputted into a structural analysis numerical model. According to various  
67 investigations (Brenner, 2005; Hinks *et al.*, 2012), the geometric models can be described by: a) a  
68 boundary representation, in which the geometric model represents the masonry structure explicitly; b)  
69 constructive solid geometry (CSG), in which the geometric model represents the masonry structure  
70 from Boolean operations of simpler geometric objects; and c) spatial enumeration, in which the

71 geometric model of the masonry structure is represented as a composition of smaller geometric models  
 72 occupying the domain of the masonry structure, e.g. voxels.

73 Evidence from past studies (Heyman, 1969) has shown that geometric changes in masonry structures  
 74 can greatly influence their mechanical response. Following this intuition of Heyman, numerous  
 75 investigations, it has been shown that the variation in the geometry on a block-based level (i.e. joint  
 76 inclination, block size and bond pattern) causes significant differences in the predicted structural  
 77 behaviour of a masonry structure to be analysed, see

78 Table 1. Notably, Szakály *et al.* (2016) demonstrated that the variance in masonry bonding pattern  
 79 yielded significant influence on both failure mode and collapse load of the masonry wall panels. In  
 80 another study (Godio *et al.*, 2018), found that the arrangement and size of blocks are significantly  
 81 influential on the out-of-plane capacity of wall panels subjected to seismic loading. The same year,  
 82 Forgács *et al.* (2018), also found that the construction method of masonry arches with the same span  
 83 and same angle of skew significantly influences the collapse load and failure mode of the arches.  
 84 Finally, in a more recent study (Napolitano and Glisic, 2019), found that the block pattern significantly  
 85 influences the structural capacity of wall panels with the same height and length.

86 *Table 1. The effect of geometric uncertainty of ad-hoc geometric models on structural behaviour.*

Study	Geometrical properties investigated	Structural behaviour indices investigated	Main findings
(Szakály <i>et al.</i> , 2016)	Masonry wall patterns	Shear resistance of masonry wall due to horizontal point load	Vertical bricks affect shear resistance for low confining vertical loads
(Godio <i>et al.</i> , 2018)	Block size, bed joint orientation	Collapse load due to horizontal gravitational load	The larger the blocks, the higher the structural capacity. The bed joint angle also influences structural capacity
(Forgacs <i>et al.</i> , 2017)	Block size, block length-to-width ratio (L/H)	Stability due to self-load	The larger the blocks (the larger the L/W for constant W), the more stable the arch is
(Forgács <i>et al.</i> , 2018)	Masonry arch construction methods	Collapse load due to vertical point load	The method of construction (false skew, helicoidal or logarithmic) influenced the structural capacity of masonry arches
(Pulatsu <i>et al.</i> , 2018)	Masonry arch block bond pattern and layer number (ring number)	Collapse load due to vertical point load	Double-layer arch had a lower structural capacity of the respective single. Bond pattern of arch voussoirs was not influential on structural capacity
(Napolitano and Glisic, 2019)	Bonding course of masonry walls	Maximum vertical displacement and principal stress due to settlement	The consideration of bonding courses increased structural capacity for settlement

87 Although from the above studies (see Table 1) it is evident that the employment of simplified (i.e. ad-  
88 hoc or idealised) geometric models can significantly compromise the robustness of the structural  
89 analysis, the reasons why the majority of numerical modelling studies focusing on employ simplified  
90 geometric models are: a) difficulties in geometric data acquisition, i.e. obtaining the exact location of  
91 each block and joint (geometry on a block-based level) manually is an extremely laborious procedure,  
92 and potentially prohibitive for the case of a large-scale structure; b) developing accurate geometric  
93 model development is extremely complex (i.e. the block-by-block procedure (Sarhosis *et al.*, 2016c) in  
94 comparison with the user-friendly continuum-based models as will be discussed in the forthcoming  
95 sections), while methodical and automated frameworks for such task lack; and c) comprehensive  
96 investigation still lacks on the automation of the process from surveying to geometric model  
97 development for the numerical modelling of masonry structures. Of major importance to the geometric  
98 model development process is the numerical method employed i.e. continuum or discontinuum  
99 approach (Bobet *et al.*, 2009). Within continuum methods, the discontinuities may be implemented  
100 either implicitly or explicitly. Conversely, in discontinuum methods, discontinuities in masonry are  
101 explicitly incorporated.

102 Over the last two decades, advances in non-contact sensing techniques such as terrestrial laser scanning  
103 (TLS) and Structure-from-Motion (SfM) photogrammetry have started to drastically change the  
104 building industry due to such techniques rapidly and remotely harvesting digital geometric records of  
105 objects and features in a point cloud format. SfM photogrammetry is a passive non-contact sensing  
106 technique in which, interest points (IPs) are detected in overlapping images of a structure and used to  
107 reconstruct a point cloud using common feature matching and triangulation (Westoby *et al.*, 2012).  
108 Compared to SfM photogrammetry, TLS is an active non-contact sensing technique. Time-of-flight  
109 scanners, which are more relevant to applications of masonry structures, measure distance by timing  
110 the emission of a pulse of laser energy to the detection of the reflected signal (Mills and Barber, 2004).  
111 Both SfM photogrammetry and TLS have a demonstrated suitability for accurately and rapidly  
112 obtaining the complex geometry of masonry structures (Altuntas *et al.*, 2017; D'Altri *et al.*, 2018b).

113 The aim of this paper is to review approaches for the employment of non-contact sensing to enhance  
114 both the efficiency and reliability of numerical modelling of historic masonry. Firstly, the numerical  
115 modelling approaches of historic masonry structures are reviewed, with emphasis on those with the  
116 potential to perform high-level structural analysis. Following, non-contact sensing techniques  
117 approaches are reviewed for surveying masonry structures, concerning their accuracy and cost-  
118 effectivity. Finally, approaches of developing geometric models from the data of structural surveying  
119 are reviewed with respect to their degree of automation and facility in implementation. The organization  
120 of this paper is as follows: Section 2 introduces masonry as a construction material; Section 3 presents

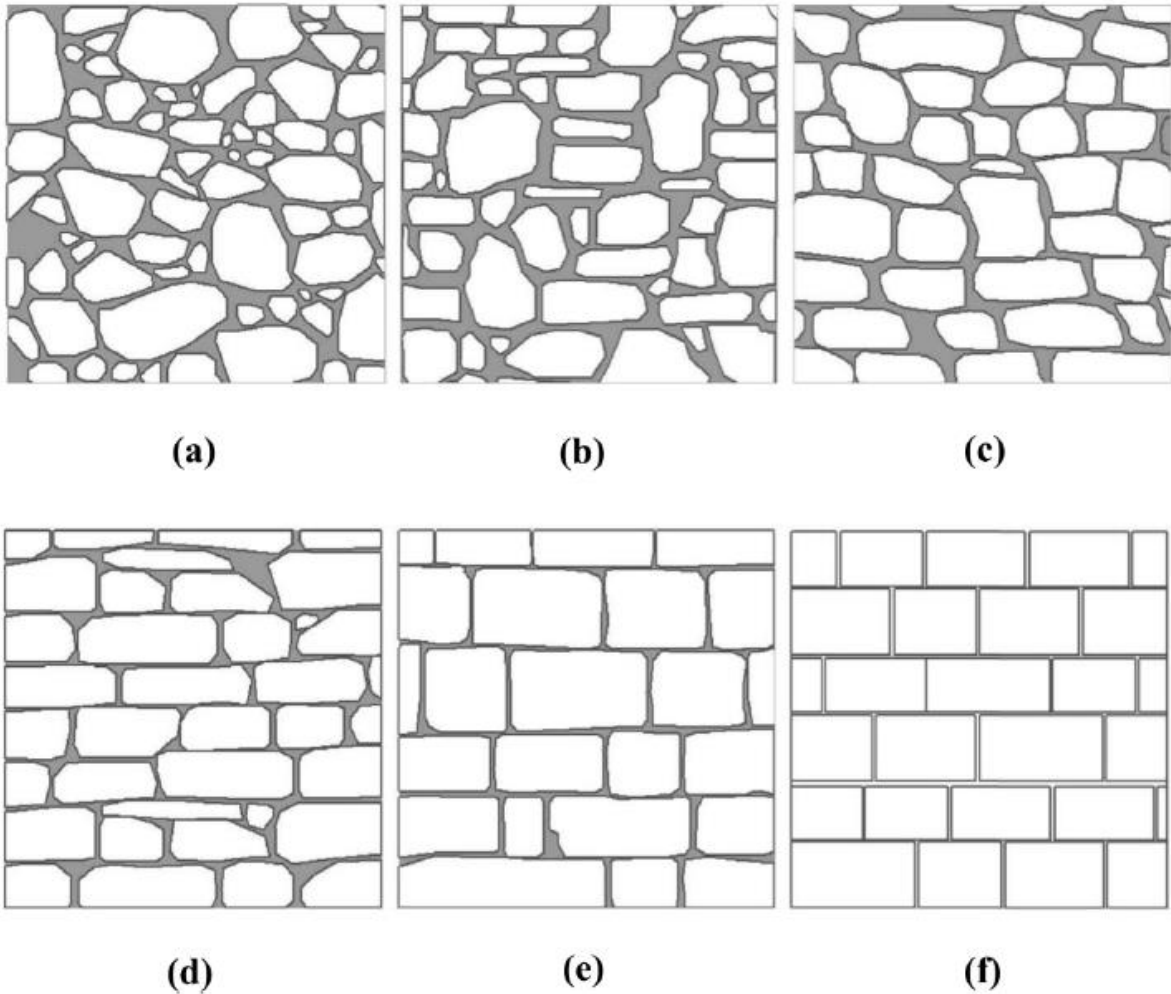
121 numerical modelling strategies of masonry; Section 4 reviews current high-level numerical modelling  
122 approaches; Section 5 reviews non-contact sensing techniques for capturing geometric data for  
123 numerical modelling; Section 6 reviews geometric model development strategies for automating  
124 numerical modelling; and Section 7 reports the paper's conclusions.

## 125 **2 Masonry as a construction material**

126 Masonry is one of the oldest construction materials, still widely adopted in a similar manner to that of  
127 thousands of years ago (Lourenco, 1996). In the 19th century, the appearance of building materials such  
128 as steel and reinforced concrete have led to its reduction to either load-bearing walls of small-scale  
129 buildings or mere infill walls (Hendry, 2001) yet historic masonry structures encompass a considerable  
130 proportion of the built environment. While masonry is highly effective for sustaining vertical  
131 compressive (Heyman, 1997; Como, 2013), it is susceptible to sustain tension and shear loads. Masonry  
132 is generally a highly durable form of construction. However, the materials used, the quality of the mortar  
133 and workmanship, and the pattern in which the units are assembled can substantially affect the durability  
134 of the overall masonry construction.

135 The art of construction by assembling units of stone, clay, brick, or concrete blocks defines masonry.  
136 Masonry is classified based on the spatial organisation of its units, the so-called masonry typology,  
137 which also significantly influences masonry's structural behaviour (Zhang *et al.*, 2018a). Brick  
138 masonry, for instance, can be distinguished into periodic (similar to stone ashlar, in which the pattern is  
139 termed bond) and rubble. On the other hand, stone masonry has been classified (Vanin *et al.*, 2017) by  
140 various levels of regularity, such as: a) irregular stone masonry, with pebbles, irregular stone units  
141 (Figure 1a); b) uncut stone masonry (Figure 1b); c) cut stone masonry with good bonds (Figure 1c); d)  
142 soft stone regular masonry (Figure 1d); e) ashlar masonry, built with sufficiently resistant blocks (Figure  
143 1e); and ashlar masonry, built with sufficiently resistant blocks and the blocks are perfectly rectangular  
144 and all blocks of one row have the same height (Figure 1f).

145 Of major importance to the structural behaviour of masonry is also the cross-section morphology (Binda  
146 *et al.*, 2009). For masonry walls, for instance, this may be: a) single leaf; b) double leaves without  
147 connection; c) double leaves with connection; and treble leaf stone masonry walls. This aspect is  
148 important due to its influence on the monolithic behaviour of the masonry (Binda *et al.*, 2009). Finally,  
149 the type of structure masonry also significantly affects its structural behaviour.



150

151 *Figure 1: Typologies of stone masonry (Vanin et al., 2017): (a) class A; (b) class B; (c) class C; (d) class D; (e)*  
 152 *Class E1; and (f) Class E2.*

153 **3 Numerical modelling strategies**

154 Depending on the required accuracy and detail required of the structural analysis, multiple modelling  
 155 strategies have been proposed by various investigators (Lourenco, 2002; Asteris *et al.*, 2015; D’Altri *et*  
 156 *al.*, 2019). Modelling strategies are distinguished according to how heterogeneity of masonry is  
 157 simulated in a given numerical model. According to a recent classification (D’Altri *et al.*, 2019), the  
 158 following modelling strategies can be employed: a) continuum models; b) block-based models; c)  
 159 macro-element models; and e) geometry-based models.

160 **3.1 Continuum models**

161 In this strategy, the structure is considered as a homogenous anisotropic continuum which is effective  
 162 for instances where the anisotropy of masonry is less significant (D’Altri *et al.*, 2019) such as the case  
 163 of rubble masonry structures. The main advantages of continuum modelling, in comparison with block-

164 based modelling are: a) the anisotropy of the masonry is not explicitly represented with a block-by-  
165 block manner, which significantly simplifies geometric model development (as will be further detailed  
166 in Section 4.1); and b) since the geometric refinement is reduced, the computational burden is  
167 significantly reduced accordingly. However, a major limitation of this strategy is that the determination  
168 of material properties is an extremely complicated task; which is accomplished through either the  
169 employment of experimentally derived constitutive laws or homogenisation processes. Furthermore,  
170 another limitation is that only knowledge of global behaviour is emphasised whilst the local behaviour  
171 (i.e. interaction between blocks) is neglected.

### 172 **3.2 Block-based models**

173 In the block-based modelling strategy, the masonry blocks and joints are explicitly described within the  
174 geometric model as blocks and mortar elements. Due to this very detail, a simplified variation of the  
175 block-based modelling is usually employed in which the blocks are expanded to maintain the initial  
176 geometry and mortar is replaced with a zero-thickness element. This is particularly advantageous for  
177 regular masonry structures (and generally low bond strength masonry), where the anisotropy of the  
178 masonry is well-defined (D'Altri *et al.*, 2019) and failure predominantly occurs due to sliding and  
179 cracking between blocks. Furthermore, the Young's modulus, Poisson's ratio, and inelastic properties  
180 of both the masonry block and mortar are accounted for. The main advantages of the block-based  
181 modelling strategy are: a) it enables a realistic description of a given masonry structure, with an explicit  
182 representation of the masonry's anisotropy and structure's geometric details; b) it facilitates the  
183 capturing of accurate structural behaviour and failure modes; and c) mechanical properties can be  
184 derived straightforwardly, directly from small-scale experiments. However, its limitations are also  
185 notable, such as that: a) it can be computationally burdensome, especially for the case of large-scale  
186 masonry structures; b) the development of geometric models is extremely cumbersome which can also  
187 severely delay the given numerical modelling approach (as will be further detailed in Section 4.2); and  
188 c) it is only employed in research except for few high-level practising engineers (D'Altri *et al.*, 2019).

### 189 **3.3 Macro-element models**

190 In this strategy, the masonry structure is considered as an assembly of structural components, typically  
191 piers and spandrels (vertical and horizontal load-bearing elements respectively). Within the geometric  
192 model, spandrels and piers are assigned based on experimental knowledge of the modelled structure.  
193 Regarding material properties, a constitutive law is employed that governs the structural behaviour on  
194 a spandrel and pier level. Owing to this simplicity, the main advantages of the macro-element modelling  
195 strategy is its low computational burden which makes it of the most employed for the dynamic analysis  
196 of unreinforced masonry (URM) (D'Altri *et al.*, 2019). However, it has significant limitations, such as:

197 a) the initial predefinition of the spandrels and piers appears to be oversimplified which necessitated  
198 judicious application; and b) the local behaviour associated with the anisotropy of masonry cannot be  
199 accounted for.

### 200 **3.4 Geometry-based models**

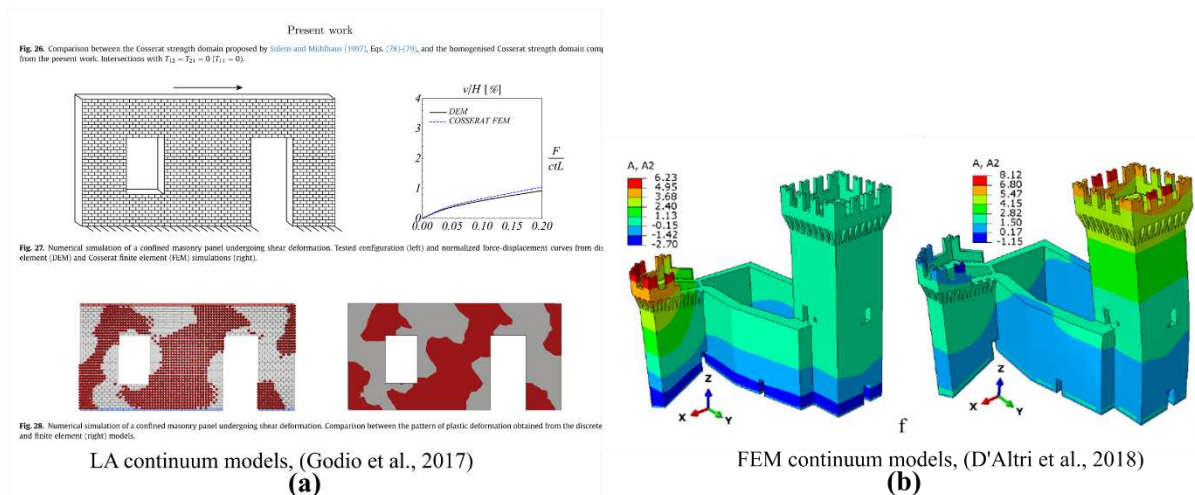
201 In this strategy, further, than the loading scenario, the only other variable is the geometric model which  
202 is described as a rigid medium. Such models typically employ limit analysis (LA) approaches and lead  
203 to the estimation of the collapse or equilibrium load through the lower and upper boundary theorems  
204 respectively. The main advantage of this strategy is its simplicity in implementation and low  
205 computational burden (D’Altri *et al.*, 2019). However, the limitation of such models is associated with  
206 their simplicity (i.e. the only variables being geometry and loading), which does not permit an in-depth  
207 understanding of the structural behaviour of masonry. Furthermore, they share the inherent limitations  
208 of the LA models which is the fact that they only provide the collapse load and failure mechanism.

## 209 **4 High-fidelity numerical modelling approaches**

210 In this Section, the current state-of-the-art of numerical modelling approaches are reviewed. Due to the  
211 large volume of existent research on the numerical modelling of masonry, a comprehensive review of  
212 all the literature would be unrealistic. Thus, the current Section is limited to the two most advanced  
213 strategies (i.e. high-level) which are the continuum and block-based, according to D’Altri *et al.* (2019).  
214 The interested reader is however referred to further literature (Roca *et al.*, 2010; Smoljanovic *et al.*,  
215 2013b; Asteris *et al.*, 2015; Sarhosis *et al.*, 2016c; Baraldi *et al.*, 2017; Ademovic and Hadzima-Nyarko,  
216 2019; D’Altri *et al.*, 2019).

### 217 **4.1 Continuum models**

218 Within the continuum models, the following approaches have been identified: a) LA continuum models;  
219 and b) finite element method (FEM) continuum models. The following paragraphs introduce both the  
220 approaches and relevant studies, as demonstrated in Figure 2.



221

222 *Figure 2: Continuum-based models.*

223 **4.1.1 LA continuum models**

224 LA models are well-established for the structural analysis of masonry structures. The main advantage  
 225 of such models is that they provide the masonry structure's collapse load and failure mode, rapidly with  
 226 a relatively little computational demand in most cases. For this very reason, they are particularly  
 227 attractive to practising engineers through their availability within various commercial software  
 228 packages such as *Ring* (LimitState, 2019). However, a significant limitation is that only the collapse  
 229 load is provided whilst failure displacements are unknown (i.e. load-displacement type responses are  
 230 unattainable). Furthermore, the assumptions the LA employs, especially concerning material properties  
 231 can be oversimplified.

232 A first class of LA models were developed within the continuum modelling strategy. In the so-called  
 233 direct-continuum models, the macroscopic constitutive law ascribed to the numerical model is derived  
 234 directly from experiments. For instance, *Milani et al. (2012)* developed direct continuum models of a  
 235 full-scale historic masonry tower, employing a piecewise linear approximation with a Mohr-Coulomb  
 236 failure criterion and tension cut-off and cap in compression for masonry interfaces. Concerning the  
 237 solution, linear programming was employed. A second approach is based on the homogenisation theory;  
 238 in which masonry is represented with a periodic regular texture while the macroscopic constitutive law  
 239 is obtained from the solution of a boundary cell problem in at a cell level. Within this approach, *Milani*  
 240 *et al. (2006a)* presented a pioneering investigation with homogenisation within the LA, by employing  
 241 the polynomial expression of the stress field inside a representative volume element (RVE) whilst the  
 242 structural capacity of masonry was deduced by utilizing the strength domain. Many state-of-the-art  
 243 studies have subsequently followed with advanced homogenisation approaches (*Milani et al., 2006b*;

244 Cecchi *et al.*, 2007; Cecchi and Milani, 2008; Milani, 2011; Cavalagli *et al.*, 2013; Godio *et al.*, 2017),  
245 as shown in Figure 2a.

#### 246 **4.1.2 FEM continuum models**

247 Whilst the LA is effective for an accurate prediction of the collapse load, it cannot provide a detailed  
248 structural analysis, which consists in describing the in-service and collapse behaviour. In the need for  
249 more sophisticated structural analysis than the LA, FEM continuum models have also been employed,  
250 which can provide load-displacement type responses. The main advantages of the FEM continuum  
251 models according to Sarhosis *et al.* (2016c), include:

- 252 • Straightforward implementation due to a multitude of commercial practice-oriented software  
253 packages;
- 254 • Facilitated geometric model development through user-friendly tools;
- 255 • Common application by both practising engineers and researchers.

256 The earliest class of FEM continuum models attempted to simulate masonry on a global scale through  
257 ascribing a constitutive law capable of reproducing the anisotropy of masonry. The so-called non-  
258 tension models, developed by Del Piero (1989), were built on the idealisation that masonry has a zero  
259 tensile strength. Whilst they were effective for an initiatory structural analysis, they could not be  
260 adopted for the tensile regime of masonry structures. Effectively, since actual masonry structures do  
261 possess a tensile strength (even if small), non-tension models cannot simulate the post-peak behaviour  
262 of masonry structures and lead to incorrect failure modes.

263 The necessity for capturing the non-linear behaviour of masonry led to the replacement of non-tension  
264 models with more advanced, non-linear models, inspired by the numerous smeared crack, orthotropic  
265 plasticity and orthotropic damage models of reinforced concrete (Hofstetter *et al.*, 2011; Jirásek, 2011).  
266 Lotfi and Shing (1991) pioneered the employment of non-linear models by evaluating the smeared crack  
267 model on masonry shear walls. Generally, smeared crack models are advantageous for historic masonry  
268 structures (such as rubble masonry structures) due to: a) the randomness of the masonry's geometry,  
269 the assumption of isotropy is well-standing; and b) their facility of implementation since are found  
270 within most commercial FEM codes (D'Altri *et al.*, 2019). For this reason, they are still employed to  
271 this day, as in the study of (D'Altri *et al.*, 2018) (shown in Figure 2b). However, for the case of regular  
272 masonry, especially of a low-bond strength, the assumption of orthotropy is not well-standing and  
273 smeared crack models cannot be employed.

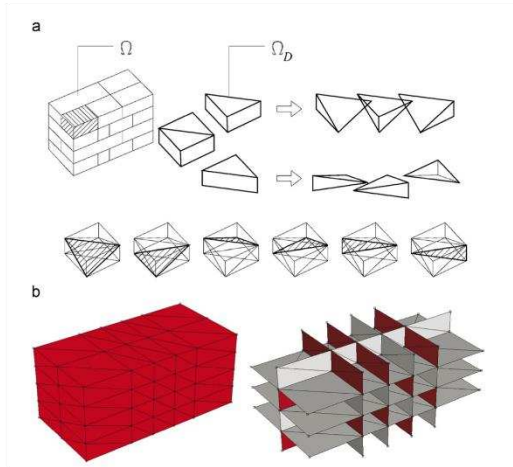
274 In an attempt to overcome the limitations of smeared crack models, Lourenco and Rots (1997),  
275 formulated the first orthotropic plasticity models which effectively represented the tensile strength of

276 the material in the principal directions. The specific models were validated in comparison with  
277 experimental masonry panels and proved extremely effective for capturing experimental behaviours.  
278 Recently, orthotropic damage models have been extensively employed, including many state-of-the-art  
279 studies. (Lopez *et al.*, 1999; Berto *et al.*, 2002; Reyes *et al.*, 2009; Pelà *et al.*, 2011; Pelà *et al.*, 2013;  
280 Pelà *et al.*, 2014).

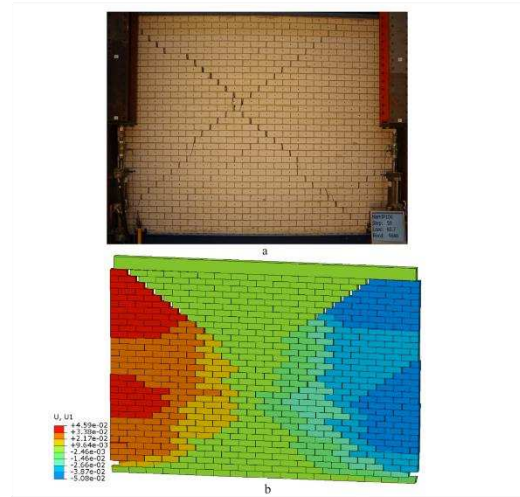
281 As with the LA, homogenisation processes have also been applied to the FEM. Pietruszczak and Niu  
282 (1992) presented an early homogenisation approach which was performed on masonry wall panels with  
283 the FEM in a two-stage manner, by introducing the head joints and bed joints as elastic inclusions and  
284 dispersed sets of weaknesses. However, Antoine (Antoine, 1995), formalised the homogenisation  
285 procedure by carrying it out in one step only, introducing the actual pane thickness and the actual brick  
286 geometry. Further on, more advanced homogenisation approaches have been developed, capable of  
287 considering complex failure mechanisms such as in (Lopez *et al.*, 1999; Zucchini and Lourenço, 2002).  
288 State-of-the-art homogenisation studies have included multi-scale approaches which overcome mesh  
289 dependency whilst representing localised failure (Leonetti *et al.*, 2018). This is carried out with a so-  
290 called first-order homogenisation until a threshold of damage is reached. After reaching the threshold,  
291 the damaged region of interest is replaced with a heterogeneous material (D'Altri *et al.*, 2019).

## 292 **4.2 Block-based models**

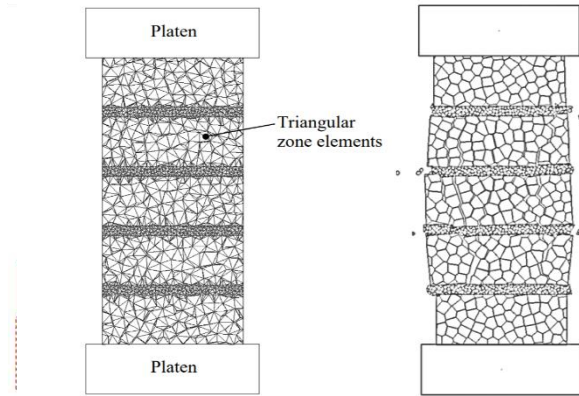
293 Within the block-based models, the following approaches have been identified: a) LA block-based  
294 models; b) FEM block-based models; c) distinct element method (DEM) models; d) non-smooth contact  
295 dynamics (NCSD) models; e) discontinuous deformation analysis (DDA) models; and e) finite-discrete  
296 element method (FDEM) models. The following paragraphs introduce both the approaches and relevant  
297 studies, as demonstrated in Figure 3.



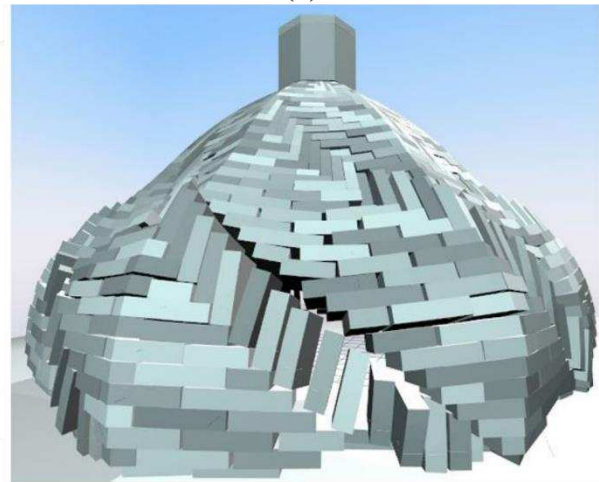
LA block-based models, (Milani, 2008)  
**(a)**



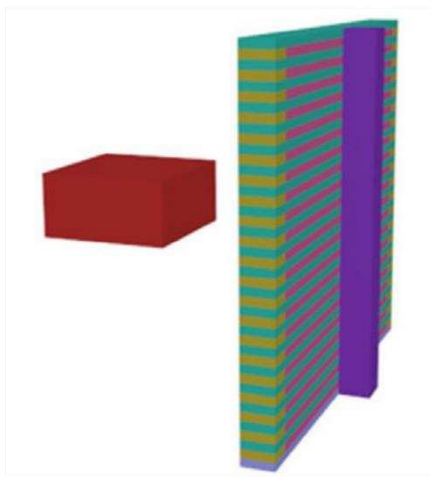
FEM block-based models, (D'Altri et al., 2019)  
**(b)**



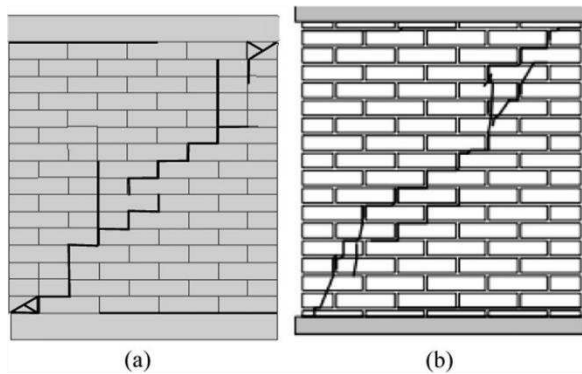
DEM models (Sarhosis & Lemos 2018)  
**(c)**



NSCD models (Beatini et al., 2018)  
**(d)**



DDA models (Liu et al., 2018)  
**(e)**



FDEM models (Smoljanovic et al., 2013a)  
**(f)**

298

299 *Figure 3: Block-based models.*

#### 300 4.2.1 Limit Analysis block-based models

301 A second class of LA models have been developed specifically for the block-based strategy. Livesley  
302 (1978) presented a pioneering lower bound LA solution for 2D masonry arches. However, due to the  
303 employed associated flow rule, two major shortcomings arose from this model: a) unreliable failure  
304 mode prediction; and b) overestimation of collapse load. Many investigators thus attempted to  
305 overcome these limitations, by implementing a non-associated flow rule. Notably, Fishwick (1996)  
306 developed a mixed lower and upper bound solution, to carry out non-associated LA of multiring arch  
307 bridges. This was through utilizing a mathematical program to solve an underlying mixed  
308 complementary problem (MCP) involving a system of orthogonal sign-constrained vectors. Despite its  
309 robustness for minimum collapse load calculation, it was effective for a small number of blocks only.  
310 Similarly, Baggio and Trovalusci (Baggio and Trovalusci, 1998; Baggio and Trovalusci, 2000)  
311 developed an MCP-like non-associated solution which attempted to find the minimum load factor by  
312 direct minimisation (with the so-called optimisation problem) under complementary constraints. This  
313 solution was also found unmanageable for structures of several blocks. Subsequently, Ferris and Tin-  
314 Loi (2001) proposed another approach for the collapse loads of discrete rigid block systems through a  
315 constrained optimisation problem known as a Mathematical Program with Equilibrium Constraints  
316 (MPEC). Orduña and Lourenço (2005) additionally employed a novel load path following procedure  
317 which yielded in the robust structural analysis of 3D masonry assemblies. Finally, in recent years, other  
318 investigators have employed more sophisticated techniques such as cone programming (Portioli *et al.*,  
319 2014) to carry out the non-associated LA.

320 Despite the effectivity of non-associated LA models for the analysis of masonry, two disadvantages are  
321 made apparent here: a) they all assume infinitely resistant bricks which permits plastic dissipation at the  
322 interfaces; b) the combination of a non-tension and rigid block can lead miscalculation of the failure  
323 load (Milani, 2008). Thus, another group of investigators, have employed the so-called finite element  
324 limit analysis (FELA), without resorting to a non-associative flow rule. In a pioneering study, Sutcliffe  
325 *et al.* (2001) developed a novel lower bound finite element limit analysis (FELA) solution to calculate  
326 collapse loads of unreinforced masonry shear walls. The solution was derived from the imposition of  
327 equilibrium with appropriate yield and stress boundary conditions. Later on, another FELA approach  
328 was also presented, however with an upper bound solution (Milani, 2008), as shown in Figure 3a. This  
329 included interfaces with a Mohr-Coulomb failure criterion, a tension cut-off and cap in compression for  
330 mortar joints in combination with a Mohr-Coulomb failure criterion for bricks, enabling complex failure  
331 modes (such as masonry crushing) to be captured. Other studies have also followed this approach  
332 (Milani, 2008; Milani *et al.*, 2009). Finally, the upper bound FELA has also been applied to the 2D  
333 static analysis of large-scale structures such as masonry arch bridges (Cavicchi and Gambarotta, 2006).

#### 334 4.2.2 FEM block-based models

335 A significant scientific intent has also been devoted to the development of FEM models capable of  
336 block-based modelling. Page (1978) pioneered the so-called textured continuum approach, in which the  
337 discontinuities of masonry are represented implicitly by locally altering the texture of the mesh,  
338 corresponding to the mortar. Whilst many studies have the textured continuum approach (Ali and Page,  
339 1988; Addessi and Sacco, 2016; Petracca *et al.*, 2017; Serpieri *et al.*, 2017), a significant limitation is  
340 the implicit representation of discontinuities (based on a continuum). This can primarily make it  
341 difficult to capture specific failure modes (e.g. sliding and separation of blocks) and secondarily  
342 computationally expensive to implement.

343 Another group of FEM block-based models involve the explicit representation of masonry's  
344 discontinuities through zero-thickness interfaces. This so-called interface element approach was  
345 formulated by Lotfi and Shing (1994). Later on, the pioneering study of Lourenco and Rots (1997)  
346 greatly improved the interface approach with the so-called multi-surface models in which, the  
347 structure's damage was gathered at the interfaces only, permitting a notably increased efficiency of  
348 structural analysis. Recently, owing to the effectivity of the multi-surface models, they have been  
349 enhanced by other investigators, particularly for masonry wall panels (Gambarotta and Lagomarsino,  
350 1997; Macorini and Izzuddin, 2011; Chisari *et al.*, 2018). Another confirmation of their effectivity is  
351 that they are of the few FEM block-based models which have been successfully employed for full-scale  
352 masonry structures such as bridges (Zhang *et al.*, 2016; Zhang *et al.*, 2017; Zhang *et al.*, 2018b; Tubaldi  
353 *et al.*, 2019). However, here, a setback of the approach is also made apparent in the fact that, especially  
354 for the case of full-scale structures, they appear computationally burdensome, necessitating high power  
355 computational (HPC) facilities.

356 Whilst the interface approach is highly-effective, the representation of complex behaviours such as the  
357 crushing of masonry is still a challenge, since numerical properties cannot be obtained with ease.  
358 Attempting to overcome such difficulties, an innovative research group (D'Altri *et al.*, 2018a; D'Altri  
359 *et al.*, 2019) introduced a novel, so-called contact-based approach within a FEM framework (within the  
360 commercial software *Abaqus* (Simulia Inc., 2017)). Specifically, contact-based interfaces were coupled  
361 with 3D non-linear-damaging textured blocks to explicitly represent the mortar and masonry,  
362 representing one of a handful of detailed block-based models available in the literature. In the initial  
363 investigation (D'Altri *et al.*, 2018a), the approach was proposed and implemented on experimental  
364 panels and validated, for quasi-static loading. In the follow-up study (D'Altri *et al.*, 2019), the approach  
365 was implemented (Figure 3b) for cyclic loading on a full-scale experimental terraced house, yielding  
366 unprecedented results for a FEM model such as large displacements (i.e. 50 mm), crushing effects and

367 manageable computational times. Additionally, material properties were derived directly from small  
368 scale experiments.

### 369 **4.2.3 DEM models**

370 Despite the apparent suitability of the FEM block-based models to simulate the heterogeneous nature  
371 of masonry, the state-of-the-art approaches such as the aforementioned interface approaches appear to  
372 still be generally computationally expensive, and in some case necessitating HPC resources.  
373 Furthermore, the more recent, innovating contact-based approaches, are also evidently suitable for the  
374 block-based modelling of masonry, and computationally manageable, however, have only found a small  
375 application which means their employability and efficiency is still questionable. In an attempt to  
376 overcome such difficulties, researchers have been attracted to discontinuum numerical methods, which  
377 have been effectively employed for the block-based modelling of full-scale masonry structures, such as  
378 masonry arch bridges, temples and churches.

379 Of the most diffused discontinuum methods employed is the distinct element method (DEM), initially  
380 developed for problems of sliding and crashing rocks (Cundall, 1971). The abbreviation DEM will  
381 herein be used interchangeably for both discrete element method and distinct element method. The main  
382 advantage of the DEM, as any such discontinuum method, is that discontinuities can be explicitly  
383 implemented into the numerical model and also handled efficiently during the simulation. Another  
384 advantage is that, like the FEM, it can capture both the in-service and collapse behaviour of the masonry.  
385 However, at the present moment, the DEM also has limitations (Sarhosis *et al.*, 2016c), including:

- 386 • A high-computational cost (which is, however, lower than that of a FEM block-based model);
- 387 • Its inherent need for block-based geometric models;
- 388 • Its limited employment to academia only at the present moment.

389 Also, of major interest to the numerical modelling of masonry are the conditions which define the DEM  
390 (Cundall and Hart, 1992), which are:

- 391 a) Finite (e.g. large) displacements and block rotation and detachment can be followed in an  
392 evolutive analysis;
- 393 b) Formation of new contact can be accounted for;
- 394 c) Block detachment is permissible.

395 The first condition ensures that the complex failure mechanisms of masonry can be captured whilst the  
396 second condition that arbitrary damage and post-peak behaviours can be efficiently simulated without  
397 the need of predefinition (Sarhosis *et al.*, 2016c).

398 Here a significant aspect of the discontinuum methods such as the DEM is made apparent, which is the  
399 contact type. This may be either the “soft contact” approach (also termed force-displacement  
400 formulation) or “hard contact” one. Essentially, the soft contact means that for two given deformable  
401 blocks, interpenetration is permitted by employing the assumption of elasticity to derive the normal  
402 stiffness. Conversely, hard contact implies that only shear movement and opening can occur (Cundall  
403 and Hart, 1992). According to Lemos (2007), the soft contact approach is preferable for the masonry  
404 where the shear and sliding forces significantly influence contacts forces in masonry structures.

405 The fact that DEM models are the most diffused discontinuum method employed in masonry is most  
406 likely owed to the existence of two commercial software packages, *UDEC* and *3DEC* (Itasca, 2019a;  
407 Itasca, 2019c). It is, however, important to note that other software also implements the DEM, such as  
408 the commercial software package *PFC* (Itasca, 2019b), also developed by Cundall (Cundall and Strack,  
409 1980) and the open-source code *YADE* (Šmilauer *et al.*, 2010). As opposed to *UDEC* and *3DEC*, both  
410 the former employ spherical elements and have seldomly been employed for masonry.

411 Of the earliest studies with the DEM on masonry was by Dialer (1992) to investigate the shear strength  
412 of wall panels within *UDEC*. In recent years, extensive research has followed on masonry wall panels.  
413 For instance, many studies have focused on the methodical definition of material properties employing  
414 both optimisation and stochastic methods (Sarhosis and Sheng, 2014; Sarhosis *et al.*, 2020). Another  
415 innovating contribution paved the way for the detailed block-based modelling within the DEM  
416 (Sarhosis and Lemos, 2018) by employing with Voronoi blocks to explicitly represent the mortar. It is  
417 of interest to note that this was also extended to 3D Voronoi blocks in *3DEC* (Pulatsu *et al.*, 2019), as  
418 shown in Figure 3c.

419 Given the DEM’s effectivity and efficiency, it has also been widespread for masonry arch bridges.  
420 Lemos (1995) was of the earliest to carry out a 3D structural analysis of full-scale, masonry arch bridge  
421 in *3DEC*. In a later study (Jiang and Esaki, 2002), the influence of weakened material properties of an  
422 ancient bridge in Japan was assessed. Many more studies have followed on masonry arch bridges,  
423 however more recently, the research community has focused its concerns on addressing the complex  
424 soil-structure and spandrel wall behaviour of masonry arch bridges. For this aim, Sarhosis *et al.* (2019)  
425 employed Voronoi blocks to represent the soil, finding a good agreement with experimental studies.  
426 Finally, Forgács *et al.* (2019) also addressed the complex failure mechanisms of spandrel walls.

427 The DEM has also been extensively employed for the dynamic analysis behaviour of ancient temples  
428 and colonnades. Psycharis *et al.* (2003) carried out a 3D dynamic analysis of part of the ancient  
429 Acropolis in Athens with *3DEC*. Through this research, potential remediation strategies by reinforcing  
430 the temple with steel were considered. In the same spirit, many more investigations followed on ancient

431 temples, incorporating more complex geometrical details and arbitrary loading scenarios (Psycharis *et*  
432 *al.*, 2013; Stefanou *et al.*, 2015; Bui *et al.*, 2017; Tavafi *et al.*, 2019). Finally, it must be noted that  
433 plenty of other studies have also focused solely on the dynamic behaviour colonnades such as in  
434 (Sarhosis *et al.*, 2016a; Sarhosis *et al.*, 2016b; Pulatsu *et al.*, 2017).

#### 435 **4.2.4 NSCD models**

436 Whilst the DEM paved the way for employment of discontinuum numerical methods, others have also  
437 been developed with time. One such class of models belong to the NSCD, developed by Moreau (1988)  
438 which employs hard contacts and implicit time integration. In comparison with the DEM, the NSCD is  
439 advantageous in that it does not employ fictitious numerical damping (Moreau, 1988) while its implicit  
440 time integration method permits unconditionally stable solutions with larger time steps. The NSCD has  
441 been employed for masonry, however in significantly fewer studies than the DEM which could be  
442 attributed to the fact that solely one code, *LMC90* implements it (Dubois and Jean, 2003). Chetouane *et*  
443 *al.* (2005) were of the first to employ the NSCD for masonry, whilst applying the *LMC90* for the 2D  
444 structural analysis of both masonry panels and arch bridges. Amongst others, the study demonstrated  
445 the performance of the NSCD for capturing the structural behaviour of masonry in a manageable time.  
446 In another publication (Rafiee *et al.*, 2008), a 3D dynamic analysis was carried out on the Arles aqueduct  
447 in the south-east of France with *LMC90*. Further than demonstrating both the potential and efficiency  
448 of the NSCD, this pioneering study is still of a handful of full-scale dynamic analyses of masonry arch  
449 bridges in literature. Recently, the NSCD has also been particularly attractive to investigators on historic  
450 churches and domes. Beatini *et al.* (2019) implemented the NSCD within a custom-built software to  
451 assess Brunelleschi's dome in Florence, Italy. Since the actual geometry of the dome (Figure 3d) is  
452 hidden from view, various scenarios of the geometric model were considered of, octagonal and circular  
453 domes with varying bond patterns developed by a parametric function. From all the previous studies,  
454 the NSCD was demonstrated as highly-effective for efficiently capturing the complex behaviour of full-  
455 scale masonry structures.

#### 456 **4.2.5 DDA models**

457 Another group of discontinuum models is the DDA, which was developed by Shi and Goodman (Shi  
458 and Goodman, 1985; Shi and Goodman, 1989), again adopting a hard contact, implicit time integration.  
459 In comparison with the DEM, the DDA is advantageous due to its implicit time integration method, and  
460 compatibility with the FEM. Thavalingam *et al.* (2001) pioneered the employment of the DDA (as well  
461 as employing *PFC*) for the 2D quasi-static analysis of an experimental arch. Within the study, the load-  
462 displacement responses of the DDA showed good agreement with the experimental, whilst  
463 outperforming a commercial FEM code, *DIANA* (TNO DIANA BV. Delft, 2020). In recent years,

464 Perez-Aparicio *et al.* (2013) also analysed 2D arches within the DDA to examine the influence of load,  
465 voussoir number (i.e. block number) and arch embankment (i.e. the thickness of the fill above the arch  
466 crown's height). Finally, in another recent study, the DDA has also been applied to investigate the  
467 boulder impact on masonry structure in mountainous areas (Liu *et al.*, 2018). In the specific study (as  
468 shown in Figure 3e), the DDA enabled the 3D dynamic analysis of various scenarios of boulder velocity  
469 and construction type (i.e. masonry bond) to propose remediation strategies for masonry structures at  
470 risk.

#### 471 **4.2.6 FDEM models**

472 A final class of discontinuum models regard the FDEM, developed by Munjiza *et al.* (1995) employing  
473 a hard contact, implicit time integration method. Here the superiority of the FDEM is made apparent in  
474 that it is only discontinuum method that permits masonry crushing (i.e. blocks that can break and  
475 separated without the use of zero-thickness interfaces) whilst also sharing the advantages of the DDA  
476 and NSCD, in comparison to the DEM. Owen and co-workers (Owen *et al.*, 1998) were of the earliest  
477 to demonstrate the potential of the FDEM with the quasi-static 2D analysis of a full-scale masonry arch  
478 bridges whilst assessing reinforcement strategies (so-called *CINTEC* system). Amongst others, one of  
479 the model's novelties included the coupling spherical and polyhedral elements. Another more recent  
480 FDEM investigation involved the modelling of arch reinforcements (Smoljanovic *et al.*, 2015). Further  
481 than masonry arches, the FDEM has also found application in the context of cultural heritage masonry  
482 structures. Indicatively, Smoljanovic *et al.* (2013a) carried out a 2D dynamic analysis of the Prothyron  
483 in Split, Croatia. The models demonstrated the capabilities of the FDEM to capture extremely complex  
484 failure modes including cracking of the stone units, something unprecedented in block-based models  
485 (as shown in Figure 3e). Finally, as for most numerical methods within the DEM, the FDEM has been  
486 particularly attractive for the research of out-of-plane seismic loading of URM, such as (Smoljanovic  
487 *et al.*, 2018).

488

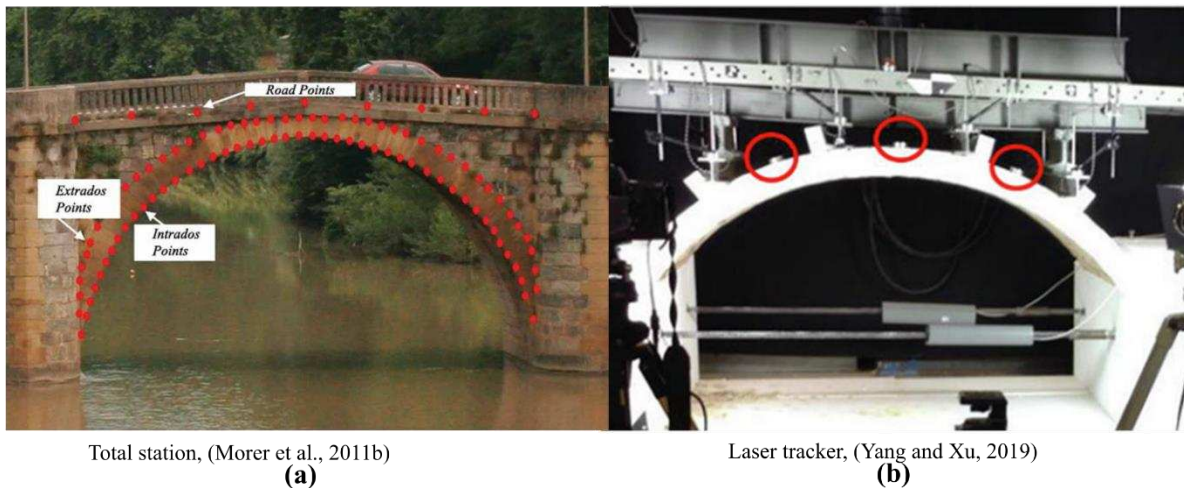
### 489 **5 Structural surveying of masonry structures for numerical modelling**

490 As found in Section 4, there is an array of approaches for high-level structural analysis of masonry  
491 structures. However as highlighted in Section 1, the majority of these studies employ simplified or ad-  
492 hoc geometric models. One reason why state-of-the-art numerical modelling approaches employ  
493 simplified geometric models is the difficulty of geometric data acquisition, owing to the employment  
494 of manual measurements (i.e. traditional geospatial techniques such as direct measurement with a tape).  
495 Nowadays, however, non-contact sensing techniques such as non-contact sensing have revolutionised  
496 many applications of civil engineering, including numerical modelling (Tang *et al.*, 2007; Chen, 2012;

497 Olsen and Kayen, 2012; Vosselman and Maas, 2014; Ye *et al.*, 2018). Of particular interest is the SfM  
498 photogrammetry pipeline which further than practical, is a considerably accurate and low-cost non-  
499 contact sensing technique (Dai and Lu, 2010). Following this intuition, this Section examines the  
500 suitability of emerging non-contact sensing techniques such as SfM photogrammetry for providing  
501 geometric data rapidly and reliably. It is noteworthy that the presented non-contact sensing techniques  
502 are classified by the author into: point-based techniques, which provide discrete points only; and cloud-  
503 based, which provide point clouds and orthoimages.

## 504 5.1 Point-based techniques

505 Within the point-based structural surveying, the following approaches have been identified as  
506 candidates for accurate geometric model development: a) total station; b) laser tracker. The following  
507 paragraphs introduce both the techniques and relevant studies, as demonstrated in Figure 4.



509 *Figure 4: Structural surveying with point-based techniques: (a) total station; and (b) laser tracker.*

### 510 5.1.1 Total station

511 A total station consists of an electronic theodolite combined with an electronic distance measurement.  
512 Through the recording of angles and points, the accurate 3D positions of discrete points are obtained.  
513 In the context of numerical modelling of masonry structures, total stations are employed to directly  
514 measure the structure (e.g., the block and joints positions) and develop a geometric model according to  
515 a given modelling strategy (e.g., with the point-based approaches of Section 6.2.1) as well as to provide  
516 control information for other non-contact sensing techniques. The main advantages of the total station  
517 are its simplicity of use and sub-cm accuracy in each direction (Morer *et al.*, 2013) which indeed makes  
518 it particularly attractive for providing control information (i.e. georeferencing ground control points),  
519 as will be demonstrated in this investigation of Figure 4a. However, the main limitation of the total  
520 station is owed its relatively high cost and to the nature of its observations (i.e. discrete points). This

521 makes its employment for the numerical modelling of large-scale structures costly and time-prohibitive  
522 due to the impractical and laborious task of measuring unmanageable numbers of blocks.

### 523 **5.1.2 Laser tracker**

524 The laser tracker is a recent technology used in large scale precision manufacturing such as aerospace  
525 and the automotive industry (Estler *et al.*, 2002). It is similar to the total station in that it is placed upon  
526 a tripod, is pointed at targets in sequence, and measures the distance to each, as well as the angles  
527 between each pair. From this raw data, full 3D coordinates of each target can be calculated. Like a  
528 robotic total station, the tracker can move itself to find the centre of the target. The tracker measures  
529 the position of a retro-reflective prism, which rather than a traditional target, is mounted in nests,  
530 permanently fixed to the structure. The prism is set in a stainless-steel sphere, such that the measurement  
531 point is at the centre of the sphere with extremely high accuracy. The nests are designed as such so that  
532 the sphere sits on three points and is held in place by a magnet, ensuring repeatability of the  
533 measurements. As is surveying with a total station, it is not possible to see all the measurement points  
534 from one instrument position which requires measurements from several positions are combined into a  
535 complete survey.

536 While the application of laser trackers is still limited in masonry structures, some pioneering  
537 investigations do exist. In one recent study, the employment of laser trackers was carried out (Barazzetti  
538 *et al.*, 2015b) to detect the static movement of the column the Cathedral of Milan. The achieved  
539 precision which was 0.1 mm, clearly demonstrated the performance of the laser tracker in such  
540 applications. In another study (Yang and Xu, 2019), laser tracking was employed for providing control  
541 information to a TLS survey of a concrete bridge, as shown in Figure 4b. Specifically, parameters of a  
542 B-spline model developed from the TLS point cloud were calibrated and validated surface accuracy in  
543 the region of 0.1 mm. These studies both demonstrate the main advantage of the laser tracker which is  
544 its accuracy, which is invaluable for providing control information. However, as the total station, it does  
545 not appear advantageous for geometric model development of large-scale structures due to providing  
546 discrete points.

## 547 **5.2 Cloud-based techniques**

548 Within the cloud-based structural surveying techniques, the following approaches have been identified:  
549 a) TLS; and b) SfM photogrammetry. The following paragraphs introduce both the techniques and  
550 relevant studies, as demonstrated in Figure 5.



TLS models, (Chen et al., 2019)  
**(a)**



SfM photogrammetry, (Chen et al., 2019)  
**(b)**

551

552 *Figure 5: Surveying with cloud-based techniques: (a) laser scanning; and (b) SfM photogrammetry.*

### 553 **5.2.1 Laser scanning**

554 At the present moment, laser scanning is one of the most important non-contact sensing techniques for  
 555 the structural surveying of masonry structures (Tobiasz *et al.*, 2019). For the so-called time-of-flight  
 556 type laser scanners which are more pertinent to this investigation, pulses of light are emitted from the  
 557 scanner's position to the masonry structure's surface whilst distance measurement results from  
 558 recording the time interval between light emission and return (Baltsavias, 1999). Typical laser scanner  
 559 components are a rotary mirror, a laser source, and a data storage module (Tobiasz *et al.*, 2019). Whilst  
 560 laser scanning provides several returns, the main product concerning numerical modelling is a dense  
 561 point cloud. Apart from 3D positions, this also includes a fourth parameter; the intensity of the returning  
 562 signal, which is particularly useful for characterizing the scanned material (Tobiasz *et al.*, 2019).

563 Laser scanning can be distinguished based upon the platform in which it is employed. When the laser  
 564 scanning is carried out from the ground, it is TLS. Whilst, when airborne platforms are employed (such  
 565 as an unmanned aerial vehicle), it is airborne laser scanning (ALS). In the context of this investigation,  
 566 TLS is more pertinent due to the scale and required accuracy of the problem. Additionally, the errors of  
 567 TLS according to Tobiasz *et al.* (2019) are summarised as: a) internal, such as instrumental errors, laser  
 568 beam errors (propagation, reflection, and refraction); and b) external errors, such as the case of the  
 569 material colour affecting the intensity, and material translucency.

570 The main advantage of laser scanning, in comparison with all the aforementioned point-based  
 571 techniques, is the rapid geometric data acquisition (e.g. M Pts level) and high-accuracy (e.g. sub-cm  
 572 level), comparable to a total station (Vosselman and Maas, 2014). For this reason, TLS is the benchmark  
 573 method of structural surveying of masonry structures, as will be demonstrated further on. However, the

574 disadvantages of TLS are found in the high cost of equipment, the necessity of multiple scan stations  
575 when oblique incidence angles occur, and in the lack of textural information provided (Peppas, 2018).

## 576 **5.2.2 Photogrammetry**

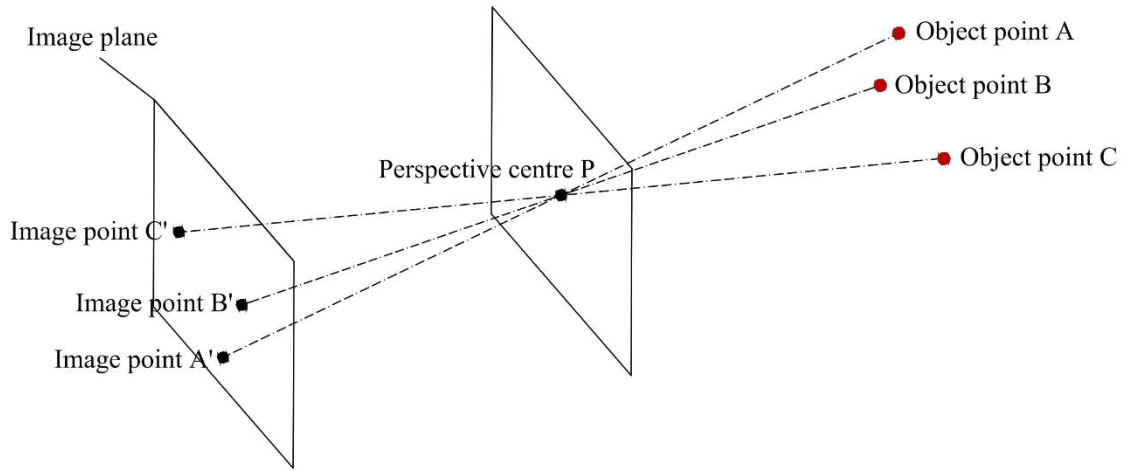
577 Photogrammetry is another commonly employed non-contact sensing technique (Tobiasz *et al.*, 2019)  
578 that deals with extracting geometric data from imagery (Wolf *et al.*, 2014). As with TLS,  
579 photogrammetry may be terrestrial or airborne according to the platform of the employed sensors. In  
580 the past, high-quality analogue metric cameras were employed in conventional photogrammetry such  
581 as in Mills and Barber (2004). Now, photogrammetry is also employed with digital cameras in  
582 combination with low-cost SfM platforms (the formulation of which will be detailed in the forthcoming  
583 paragraphs).

584 In stereo photogrammetry, which is more pertinent to this investigation, two optical rays, representing  
585 conjugate image points, ideally, intersect at an object point through a so-called spatial intersection. The  
586 establishment of the camera's internal geometry is termed interior orientation carried out by defining  
587 the interior orientation parameters (IOPs). These geometric parameters, also reported in the literature  
588 as the inner, intrinsic orientation or camera intrinsic (Luhmann *et al.*, 2006) are: a) the focal length,  
589 which is the distance between the lens centre and the lens focus point; b) the principal point (the  
590 intersection of fiducial lines); c) symmetrical radial lens; and d) the decentring distortion parameters.  
591 Relative orientation consists of the determination of the position and orientation between two images,  
592 relative to each other, resulting in the generation of a stereo model. Absolute orientation consists of  
593 defining the 3D position of control points of a stereo model in a desired coordinate system, via a 3D  
594 conformal coordinate transformation using at least two horizontal and three vertical control points. After  
595 absolute orientation, the camera's exterior orientation parameters (EOPs) are defined which are three  
596 translations and three rotations. Simultaneous multiple image orientation is determined by aerial  
597 triangulation whilst the establishment of the position and orientation of each bundle of the optical ray  
598 is termed bundle block adjustment. In the case of self-calibrating bundle adjustment such as in the  
599 software *Metashape*, re-optimisation of IOPs and EOPs are

600 The theoretical basis of photogrammetry is the so-called collinearity condition, as shown in equation  
601 (5.1), according to Dai and Lu (2010). According to this condition, any given optical ray (Figure 6) can  
602 be defined by three points: a) the image point; b) the camera perspective centre; and c) the object point.  
603 Moreover, any point of an image captured by a camera is the representation of the convergence of many  
604 optical rays (Historic England, 2017). Where  $f$  is the nominal focal length;  $(x_o, y_o)$  and  $(X_o, Y_o, Z_o)$  are  
605 the coordinates of the perspective centre in the image plane and object space, respectively;  $(x_n, y_n)$  and

606  $(X_n, Y_n, Z_n)$  are the coordinates of the  $n$ -th target in the image plane and object space, respectively;  $\lambda$   
 607 is the scale factor and  $M$  is the rotation matrix.

$$608 \begin{bmatrix} x_n - x_o \\ y_n - y_o \\ -f \end{bmatrix} = \lambda \times M \times \begin{bmatrix} X_n - X_o \\ Y_n - Y_o \\ Z_n - Z_o \end{bmatrix} \quad (5.1)$$



609

610 *Figure 6: The optical rays for object points A, B and C.*

611 SfM photogrammetry, which is of major interest to this investigation, is a recent addition to  
 612 photogrammetry which has been widely employed for the structural surveying of masonry in the latest  
 613 years. In comparison with TLS, it is advantageous due to its low-cost, facility of employment and the  
 614 high quality of its returns (e.g. high-quality RGB orthoimagery and point clouds). Additionally, SfM  
 615 photogrammetry consists of three main phases which are: a) sparse point cloud reconstruction; b)  
 616 georeferencing; and c) dense point cloud reconstruction. Sparse point cloud reconstruction regards the  
 617 process of aligning acquired images with a process of automated feature detection and correspondence  
 618 until all the photogrammetric block is oriented (Golparvar-Fard *et al.*, 2011). In specific, feature  
 619 matching firstly is carried out, which effectively finds distinct features on each image, allowing for the  
 620 automated matching across a subset of images. For example, a well-known method of carrying this out  
 621 is with the so-called Scale Invariant Feature Transform (SIFT) developed by Lowe (2004). Then, once  
 622 feature detection has been carried out throughout the dataset, quantification of the detected features  
 623 match in each image pair is carried out. The result of this process is a sparse point cloud which refers  
 624 to a point cloud of tie points. Georeferencing regards the providing of control information for the scaling  
 625 and orientation of sparse point cloud. This is commonly carried out with the use of ground control points  
 626 (GCPs) in two ways: a) indirect georeferencing, in which the points are the result of surveying; and b)  
 627 direct georeferencing, in which the obtained points are the actual camera positions (e.g. provided by  
 628 GPS or RTK). The process of georeferencing consists of recalculation of both the camera's IOPs, EOPs  
 629 resulting in a recalculated sparse point cloud coordinates which are in accordance with the control

630 information provided. This is carried out in a least-squares bundle adjustment using the information as  
631 weighted in conjunction with the tie points. Finally, once the sparse point cloud is georeferenced, the  
632 dense cloud reconstruction follows by employing a pixel disparity calculation with area-based image  
633 matching. Thereafter, pixel back-projection and triangulation (i.e. via spatial intersection) follows, in  
634 which a 3D surface is formed via gradient-based and energy minimisation algorithms to avoid  
635 irregularities.

636 As a result of the aforementioned pipeline, the main product of SfM photogrammetry is a dense point  
637 cloud, which is RGB-coloured, being a significant advantage in comparison to TLS, (which normally  
638 doesn't have RGB). However, it is to be noted that SfM photogrammetry, as opposed to TLS, does not  
639 provide the intensity data of the surveyed structure. Further than a dense point cloud, of major interest  
640 to masonry structures is orthoimagery, which may be digital elevation models (DigEMs), orthophotos  
641 or orthomosaics. Specifically, a DigEM is a mathematical description of a 3D surface in which, each  
642 grid point represents a single elevation value (Aguilar *et al.*, 2005; Wolf *et al.*, 2014) whilst the data type of  
643 DigEM is a double array of square pixels with a uniform size (Wolf *et al.*, 2014). Moreover, an  
644 orthophoto is the result of the orthorectification of DigEM and represents a continuous image grid of a  
645 uniform scale (Wolf *et al.*, 2014). The so-called orthorectification regards describing an object in its  
646 true orthographic position through the collinearity condition. Finally, orthomosaics result from joining  
647 multiple orthophotos together.

648 Also, of major importance are the errors of SfM photogrammetry, which may be due to: a) image  
649 overlap; b) GCPs; and c) external factors. The following paragraphs detail each error type. Indeed, an  
650 important aspect of acquiring images of SfM photogrammetry is the relative overlap between  
651 consecutive images. A lack of overlap has been found to cause erroneous initial image alignments and  
652 consequent erroneous sparse point cloud reconstruction (e.g. discontinuities) according to (Harwin *et al.*,  
653 2015; Dietrich, 2016). Whilst the obvious solution is though high overlap this increases the point  
654 determination redundancy (Haala and Rothermel, 2012), the computational burden can become  
655 unmanageable and thus requires consideration. Furthermore, GCP's can both decrease the systematic  
656 errors of the bundle adjustment and increase the photogrammetric abundance (Wolf *et al.*, 2014; James  
657 *et al.*, 2017). The two main factors associated with effecting the accuracy of the end-product are the  
658 GPC layout and the geometrical accuracy of the measurement GPC itself. Concerning their layout, the  
659 importance of the existence of GCPs on the border of the surveyed object has been stated on many  
660 occasions (James and Robson, 2012; Eltner *et al.*, 2016). Concerning the metric accuracy of the GCPs,  
661 it has been stated that they should be measured with an accuracy three times higher than that of the  
662 expected result (Remondino *et al.*, 2014). Finally, errors can also be associated with external factors  
663 such as image surface texture, lighting, weather conditions and instability of the camera. These such

664 factors have been attributed to affecting the SfM photogrammetry image matching algorithms (James  
665 and Robson, 2012; Remondino *et al.*, 2014) and thus causing errors.

666 Both terrestrial and unmanned aerial vehicles (UAV) -based SfM photogrammetry are well-established  
667 techniques of structural surveying of masonry structures, as summarised in Table 2. Notably, Bosché *et*  
668 *al.* (2015), surveyed walls of a historic masonry castle with the terrestrial SfM photogrammetry,  
669 yielding comparable results to TLS in terms of accuracy and point cloud density. Another study (Barrile  
670 *et al.*, 2015) investigated the performance of various SfM photogrammetry pipeline software types  
671 against a reference TLS point cloud. Of all the point clouds were generated from 219 images and three  
672 software types, *Metashape* presented the best agreement with the TLS data. In the context of the  
673 deformation analysis of historic masonry tower (Teza *et al.*, 2016), terrestrial SfM photogrammetry was  
674 also found to yield comparable results with the TLS, with errors in the range of 5-20 mm. Finally, the  
675 deformation analysis of masonry arch bridges (Soni *et al.*, 2015) also demonstrated the effectivity and  
676 accuracy of SfM photogrammetry.

677 As for many other applications of civil engineering, the use of UAVs has also grown immensely in the  
678 past decade, especially for the structural surveying of cultural heritage masonry structures. For instance,  
679 Bosché *et al.* (2015) compared the outputs of UAV-based SfM photogrammetry against those of TLS  
680 and terrestrial SfM photogrammetry for the survey of a historic castle. In this case, the UAV-based SfM  
681 photogrammetry was found to be disadvantageous, possibly due to the anteriority of the approach which  
682 lacked a methodically pre-defined flight path design. In recent years, Barrile *et al.* (2017) assessed the  
683 UAV-based SfM photogrammetry against TLS finding that the data acquisition faster, more flexible,  
684 and cost-effective but dependant on uncontrollable conditions such as weather and lighting.

685 Due to the lack of accessibility and highly irregular geometries, UAV-based SfM photogrammetry is  
686 increasingly favoured for the surveying of masonry arch bridges. For instance, one study (Bruno *et al.*,  
687 2019), combined UAV-based SfM photogrammetry and TLS for the 3D documentation of a historic  
688 bridge in Italy, leading to highly-detailed and accurate surveying, which also included textural  
689 information due to inclusion of SfM photogrammetry. In another innovating study, Pepe *et al.* (2019)  
690 captured nadir images of the intrados of a masonry arch bridge by mounting a camera (in specific a  
691 smartphone) on top of the UAV. This low-cost approach also resulted in an accurate and detailed  
692 structural surveying. Finally, in a recent study (Chen *et al.*, 2019), structural surveying of a historic  
693 aqueduct was carried out with UAV-based SfM photogrammetry to assess the performance of  
694 consumer-grade UAVs for bridge inspection (as shown in Figure 5a-b). The study demonstrated that  
695 the UAV-based SfM photogrammetry was easier to apply and more cost-effective than TLS. However,

696 problems arose, regarding non-covered areas (e.g. railings), high noise levels and low geometrical  
 697 accuracy persisted (cm-level compared to the mm-level of the TLS).

698 From the summarised studies in Table 2, it is evident that SfM photogrammetry can provide accurate  
 699 geometric data (cm-level) and rapidly (M-Pts) which is comparable to a benchmark geospatial  
 700 technique such as a total station or laser scanner. Furthermore, SfM photogrammetry can be cost-  
 701 effective due to the potential of employing of consumer-grade digital cameras. Finally, it has been  
 702 demonstrated as straightforward, which can be employed by on-site engineers with available cameras  
 703 (i.e. such as a smartphone) replacing the necessity to purposely carry survey-grade equipment (Kim *et*  
 704 *al.*, 2019).

705 *Table 2: Structural surveying of masonry structures with the terrestrial and UAV-based SfM photogrammetry.*

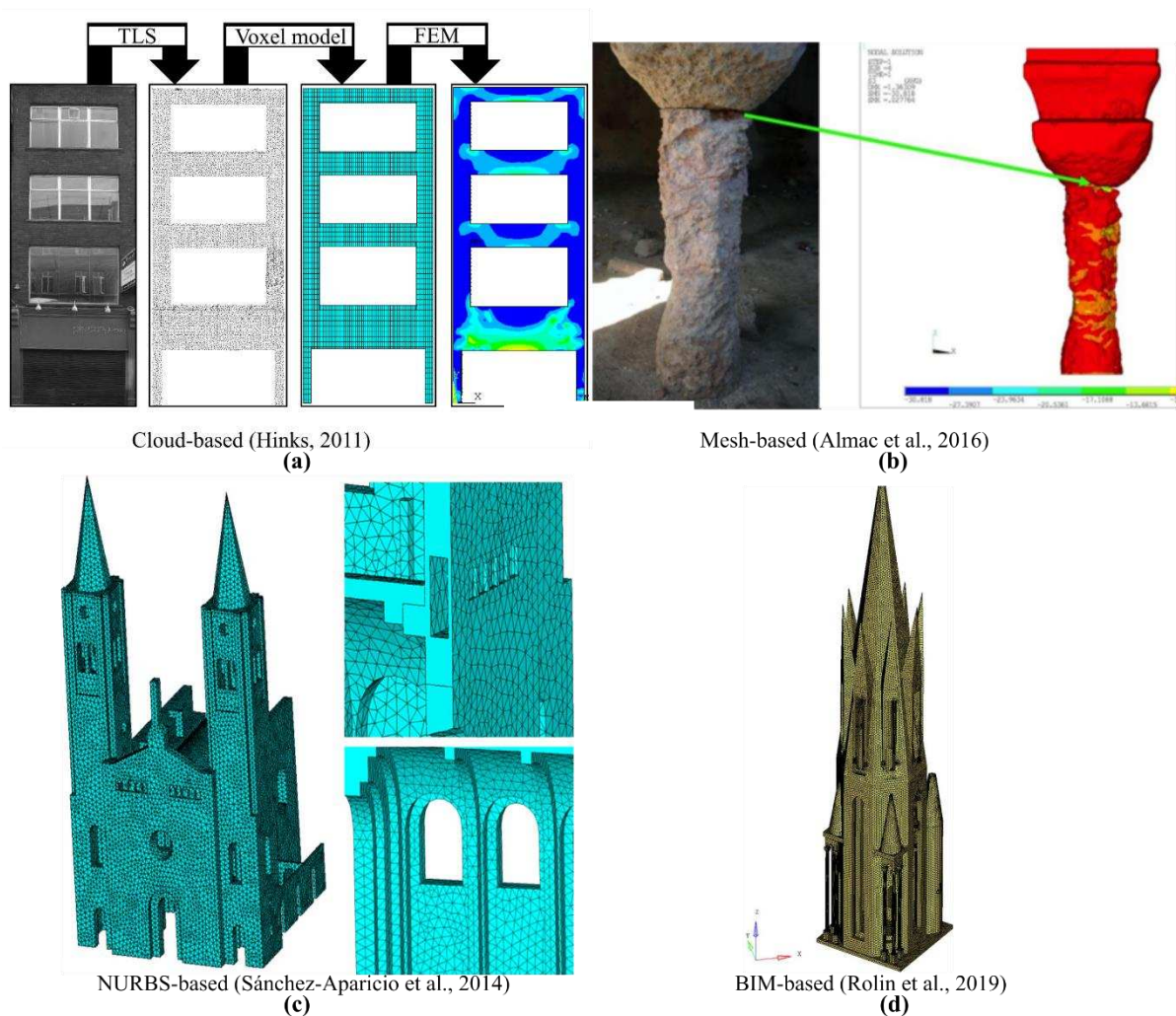
	Study	Application	Structure	Software	Image #	Dense point cloud # (M pts)	Reported GCP error (cm)	Camera
Terrestrial SfM photogrammetry	(Soni <i>et al.</i> , 2015)	Deformation monitoring	MAB	<i>Visual SfM</i>	-	-	0.1	Nikon D3200
	(Bosché <i>et al.</i> , 2015)	3D documentation	CH	<i>Metashape</i>	260	79	3	Nikon D810
	(Barrile <i>et al.</i> , 2015)	3D documentation	CH	<i>Metashape</i>	219	28.9	2	Samsung model PL20
	(Teza <i>et al.</i> , 2016)	Deformation monitoring	CH	<i>Metashape</i>	156	14.9	0.5-2	Nikon D300S
UAV-based SfM photogrammetry	(Bosché <i>et al.</i> , 2015)	3D documentation	CH	<i>Metashape</i>	460	34	3	LC Sony Alpha-7R
	(Bruno <i>et al.</i> , 2019)	3D documentation	MAB	<i>Metashape</i>	610	-	-	DJI Phantom 4 (20 Megapixel)
	(Pepe <i>et al.</i> , 2019)	3D documentation	MAB	<i>Metashape</i>	768	10	0.7	Xiaomi Mi Drone 4K UHD WiFi FPV
	(Chen <i>et al.</i> , 2019)	3D documentation	MAB	<i>Metashape</i>	295	-	-	DJI Phantom 4 (12 Megapixel)

## 706 **6 Geometric model development approaches**

707 As found in Sections 1 and 4, another reason for which the majority of state-of-the-art numerical  
708 modelling approaches employ simplified geometric models is the complex procedure of geometric  
709 model development. Indicatively, it has been found that for FEM continuum models, (which are  
710 significantly simpler than block-based), geometric model developments consumes up to 80% of the  
711 total modelling time (Zhang, 2013). To overcome this difficulty, various approaches have been adopted  
712 to automatically convert the data of various non-contact sensing techniques into geometric models,  
713 however mainly for numerical methods such as the FEM and LA. In the following paragraphs, such  
714 approaches are detailed. It is noteworthy that since few studies (Zhang, 2013; Riveiro *et al.*, 2020) exist  
715 on this relatively novel subject, the classification is proposed by the author specifically for masonry,  
716 distinguished according to the continuum and block-based modelling strategies of Section 4.

### 717 **6.1 Geometric model development for continuum modelling**

718 Within the continuum modelling strategy, the following approaches have been adopted for accurate  
719 geometric model development: a) cloud-based; b) mesh-based; c) non-uniform rational basis spline  
720 (NURBS)-based; and d) building information model (BIM)-based. The following paragraphs introduce  
721 both the approaches and relevant studies, as demonstrated in Figure 7.



722

723 *Figure 7: Geometric model development for continuum-based models.*

724 **6.1.1 Cloud-based approaches**

725 With the cloud-based approach, a point cloud is directly converted into a geometric model, usually  
 726 through spatial enumeration (Section 1), such as voxelization. The term voxelization describes the  
 727 conversion of a masonry structure’s geometric domain into an equivalent volumetric representation in  
 728 form of cuboids (voxels). The main advantage of this approach is that the structure can be of any  
 729 geometric form (i.e. non-watertight or non-convex), without the necessity of mesh generation, whilst  
 730 the volumetric modelling is achieved directly with the voxels themselves.

731 As part of his doctoral investigation, Hinks (2011) presented a pioneering voxelization approach (shown  
 732 in Figure 7a) for developing of geometric models of URM building facades. This was a novel point-  
 733 based (i.e. employing point clouds) voxelization method based on volumetric subdivision rather than

734 the previously applied methods of surface reconstruction (i.e. using meshes). Due to the anteriority of  
735 this work however, the geometric models were only two-dimensional. Based on this pioneering study,  
736 various studies employing point cloud segmentation techniques improved the 2D geometric models of  
737 the façades (Linh *et al.*, 2012; Linh and Laefer, 2013; Linh and Laefer, 2014; Truong-Hong and Laefer,  
738 2014; Iman Zolanvari and Laefer, 2016) which were all incorporated in FEM software. Castellazzi *et al.*  
739 (2015) further advanced the cloud-based approaches by developing the first three-dimensional  
740 geometric models. This was another instance of a point-based voxelization workflow which led to the  
741 full-scale FEM structural analysis of a historic masonry castle. The same particular been further  
742 employed with the structural analysis of other historic masonry structures (Bitelli *et al.*, 2016;  
743 Castellazzi *et al.*, 2017). Finally, more recently, Selvaggi *et al.* (2018) added a simplified process of  
744 geometrical assessment of the geometric models developed to the workflow. Whilst all the  
745 aforementioned studies demonstrate the cloud-based approach as efficient, they all represent the  
746 masonry as voxels, i.e., cuboids. Future cloud-based approaches should potentially consider other  
747 methods of spatial enumeration should be employed, that better approximate the anisotropic nature of  
748 masonry (for instance with Voronoi blocks, as in (Pulatsu *et al.*, 2019)).

#### 749 **6.1.2 Mesh-based approaches**

750 The mesh-based approaches refer to converting a mesh into a geometric model. Mesh herein refers to a  
751 surface mesh such as triangulated irregular network constructed from nodes of a dense point cloud and  
752 facets by Delaunay triangulation. Often, other processes precede a mesh-based approach such as  
753 watertight conversion and mesh simplification, for the structural analysis software to be able to handle  
754 a manageable amount of faces and vertices from the mesh (Riveiro *et al.*, 2020). After the surface of  
755 the structures is represented through the final mesh, it is volumetrically subdivided into either pyramidal  
756 or tetrahedral finite elements within either the structural analysis or a third-party software itself. The  
757 main advantage of the mesh-based approach is its simplicity in implication.

758 Due to its very simplicity, the mesh-based approach has been extensively applied within the context of  
759 masonry arch bridges. In an early study, Vatan and Arun (2005) developed a geometric model of an  
760 aqueduct with the mesh-based approach for structural analysis within the FEM. Later on, Arias *et al.*  
761 (2007) employed a mesh-based approach for geometric model development of a historic bridge for  
762 structural analysis within a FEM framework. This study innovatively combined data of ground-  
763 penetrating radar (GPR) to additionally determine the interior (fill) material of the bridge. Similarly,  
764 Lubowiecka *et al.* (2011) later on employed the mesh-based approach for a FEM structural analysis  
765 with a textured mesh from the SfM photogrammetry, which included the damaged areas of the bridge  
766 detected and marked, whilst GPR was again used to determine the fill of the bridge. A further study  
767 (Stavroulaki *et al.*, 2016) successfully added damage to the FEM mesh corresponding to cracks from

768 the textured mesh of SfM photogrammetry. Finally, while all the previous studies regarded single-  
769 span masonry arch bridges, Conde *et al.* (2017) developed a pioneering 3D geometric model of a full-  
770 scale, multi-span bridge for FEM structural analysis.

771 The mesh-based approach has also been applied within the context of cultural heritage masonry  
772 structures. Notably, Pieraccini *et al.* (2014) developed FEM geometric models with the use of a mesh  
773 of a historic tower. Moreover, Almac *et al.* (2016) developed FEM models of ancient columns based  
774 on a mesh obtained by TLS (shown in Figure 7b). In another study (Meschini *et al.*, 2015), FEM analysis  
775 of a fortress was also carried out using a mesh from developing a geometric model from a TLS mesh.  
776 Barrile *et al.* (2016) also followed a similar approach, however employing terrestrial SfM  
777 photogrammetry. Furthermore, Hacıfendioğlu and Maraş (2016) were of the first to employed UAV-  
778 based SfM photogrammetry to develop geometric models (FEM) of a mosque. D'Altri *et al.* (2018b)  
779 recently employed the mesh-based approach which enabled semi-automated structural analysis of a  
780 leaning tower with both FELA geometric models. Finally, more recently, Bassier *et al.* (2018) presented  
781 a mesh-based approach of which the contribution was the additional crack introduction tool, capable of  
782 adding cracks to the geometric model with manual intervention.

### 783 **6.1.3 NURBS-based approaches**

784 The NURBS-based approach is a manner of approximating a complex geometry, to facilitate its  
785 handling within the structural analysis software, whilst retaining a high degree of geometric accuracy  
786 (Riveiro *et al.*, 2020). The basis of the NURBS is the mathematical spline, a curve defined by multiple  
787 nodes (named control nodes) and polynomial functions. The simplest form of a spline is a line joining  
788 two control points. For  $n$  control points, the general rule is for polynomial function with a degree of  $n-1$ .  
789 Base Splines (B-Splines), are the subcategory of spline curves with the mathematical property of  
790 minimal support. Minimal support means that a linear combination of B-spline can be employed to  
791 express any spline function of the same degree. NURBS curve are common to B-Splines except to that,  
792 each control point has a weight; if weights were equal to 1, then the NURBS would be a B-spline. The  
793 result of a tensor product of two NURBS curves which originates from a quadrangular patch is a  
794 NURBS surface (patch). In this way, data of non-contact sensing techniques can be used as control  
795 points for retopology in a NURBS approach. It's noteworthy that the NURBS-based approach belongs  
796 to the boundary representation method of geometric model development. The NURBS approach is  
797 particularly advantageous due to providing an accurate geometrical representation of the masonry  
798 structure while requiring less manual intervention (Riveiro *et al.*, 2020). However, as with the mesh-  
799 based approach, since it represents the masonries surface only, it must be volumetrically subdivided  
800 into either pyramidal or tetrahedral finite elements within the structural analysis software.

801 Tucci and Guardini (2014) proposed a procedure of developing geometric models using a NURBS-based  
802 approach. This was carried out by applying mesh retopology within third-party software, in which the mesh  
803 was made compliant to NURBS generation. In another pioneering study (Sánchez-Aparicio *et al.*, 2014)  
804 the NURBS-based approach was used to develop a FEM geometric model (shown in Figure 7c) of a  
805 historic masonry church from the data of UAV-based SfM photogrammetry. The same research group  
806 (Sánchez-Aparicio *et al.*, 2016) carried out another structural analysis of a historic masonry structure  
807 with geometric model development carried out with the NURBS-based approach (shown in Figure 7c).  
808 Korumaz *et al.* (2017) carried out a structural analysis of a leaning minaret with the FEM with the  
809 NURBS-based approach based on TLS data. Vincenzi *et al.* (2019) used a NURBS approach to develop  
810 the geometric model of a historic tower employing combined UAV-based SfM photogrammetry and  
811 TLS data.

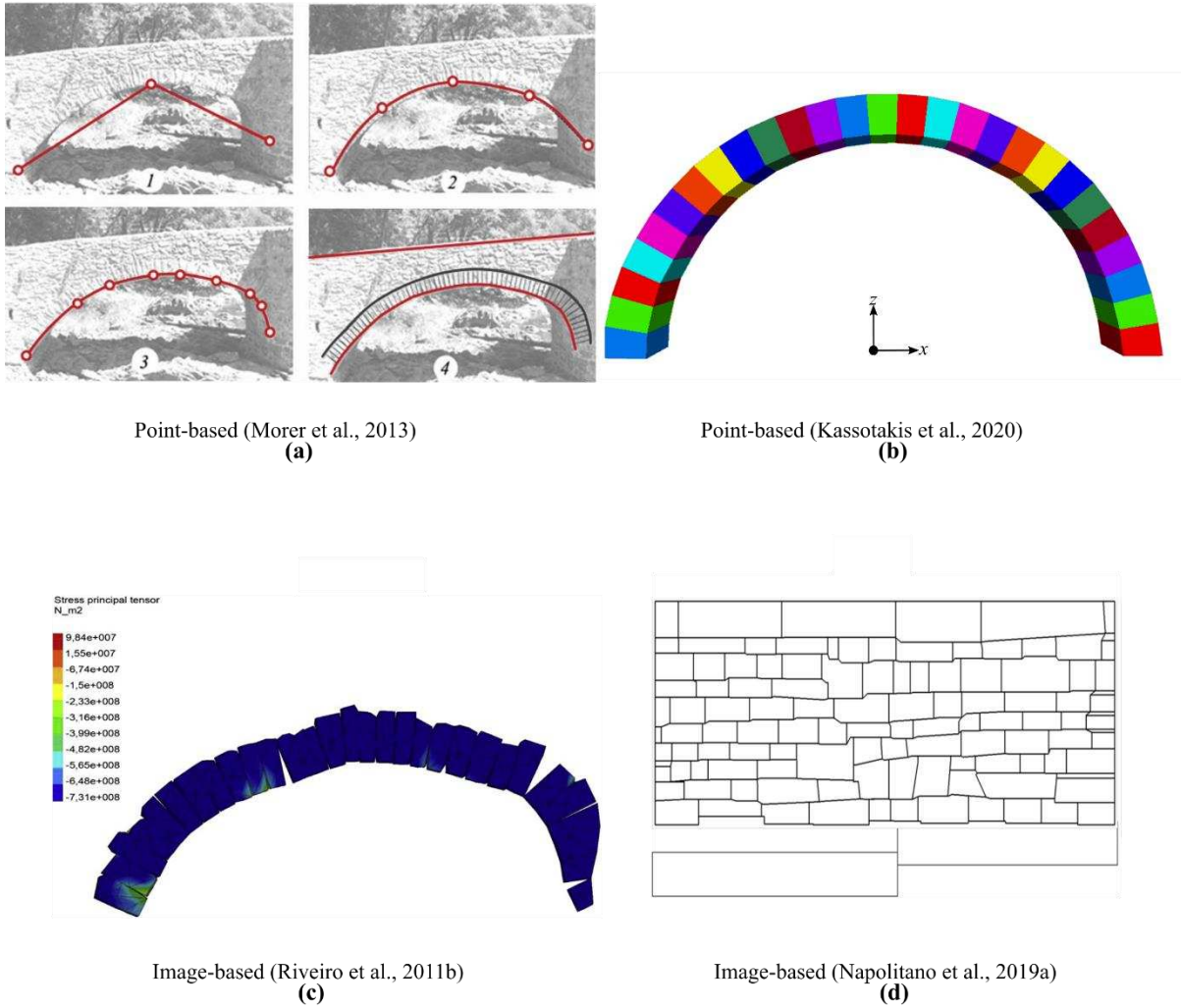
#### 812 **6.1.4 BIM-based approaches**

813 Another way of developing a geometric model is by employing a BIM. In the context of construction,  
814 the BIM is defined according to Volk *et al.* (2014) as a shared digital representation of physical and  
815 functional characteristics of a given built object which forms a reliable basis for decisions. Though  
816 BIMs are most often employed solely for documentation, in some cases, BIM models have been directly  
817 converted into geometric models for subsequent structural analysis, though on few occasions as the  
818 other approaches. In the context of cultural heritage masonry structures for instances, a pioneering  
819 investigation involving the conversion of points clouds to BIMs and BIMs to geometric models for  
820 FEM structural analysis was presented (Barazzetti *et al.*, 2015a). It must be noted that to develop the  
821 complex geometry of the church within the BIM, generative NURBS profiles were used to obtain a  
822 rigorous geometric representation of the vault, while the simple shapes were used for regular sections  
823 of the building. These procedures were carried out in a manual CAD-based environment. In a more  
824 recent study (Rolin *et al.*, 2019), a slicing method of developing BIMs from point cloud was used  
825 (shown in Figure 7d) and then the BIMs were automatically converted into FEM geometric models.  
826 Whilst the BIM approach is easy to implement, it is disadvantageous due to the lack of automation since  
827 it requires the manual development of a BIM. This, however, could be changed, owing to the vast  
828 amount of work regarding the automated conversion of point clouds to BIM, in the entitled “*scan-to-*  
829 *BIM*” approaches such as of (Andriasyan *et al.*, 2020; Bassier and Vergauwen, 2020; Bagnolo and  
830 Argiolas, 2021). Furthermore, another limitation to be mentioned is common with all the previous  
831 approaches except for the cloud-based. Effectively, even though the BIMs structural elements are  
832 explicitly represented, each element must still be volumetrically subdivided into finite elements (e.g.  
833 pyramidal or tetrahedral) within the structural analysis software.

834

835 **6.2 Geometric model development for block-based modelling**

836 Within the block-based modelling strategy, the following approaches have been adopted for geometric  
837 model development: a) point-based; and b) image-based approaches. The following paragraphs  
838 introduce the aforementioned approaches, including relevant studies as shown in Figure 8.



839

840 *Figure 8: Geometric model development for block-based models.*

841 **6.2.1 Point-based approaches**

842 A point-based approach of geometric model development implies the employment of discrete points to  
843 develop a geometric model, in a block-by-block manner. This is carried out by use of manual CAD-  
844 based software to represent the structure using the measurements of point-based non-contact sensing  
845 techniques such as a total station, or even direct measurement with a tape or a gauge. In a notable study,  
846 Morer *et al.* (2013) employed a total station to carry out numerical modelling of a masonry arch bridge,  
847 employing the block-based modelling strategy. The total station was placed in a suitable position to be

848 able to scan all the desired target points levelled, and measurement commenced (as shown in Figure  
849 8a). In the specific study, the vertices of the masonry arch's voussoirs (i.e. blocks) were measured by a  
850 total station. In a recent study, (Kassotakis *et al.*, 2020) quantified the effect of geometric uncertainty  
851 between point-based and image-based approaches (as shown in Figure 8b). The study employed tape  
852 measurements to measure the block vertices and found that point-based approaches (such as direct  
853 measurement) can be effective for small-scale structures, however unreliable geometric data can induce  
854 uncertainty into the structural analysis. Whilst point-based approaches can be adequate for small-scale  
855 structures of relatively few blocks (e.g. less than one hundred), a major disadvantage is laborious nature  
856 of both measuring discrete points and developing a geometric model from them within manual CAD-  
857 based design.

### 858 **6.2.2 Image-based approaches**

859 The image-based approach implies introducing an orthoimage of a masonry structure within a manual  
860 CAD-based framework and manually tracing the blocks and joints of the structure. Acary *et al.* (1999)  
861 pioneered the image-based approach with the structural analysis of a historic masonry structure from  
862 an orthorectified image with the NCSD. The pioneering study showed that the accurate geometric model  
863 led to a realistic failure mode of a full-scale building façade.

864 The approach has since then primarily found widespread application for masonry arch bridges. For  
865 instance, Morer *et al.* (2011) carried out the structural analysis of masonry arches with various LA  
866 approaches. Geometric models of various arches of a multi-span arch bridge were developed by  
867 manually extracting the contours of the arches from the orthoimagery of TLS. Here a limitation to the  
868 study is made apparent in that the voussoirs were not extracted from the orthoimagery, however,  
869 obtained roughly by dividing the arch contours into arbitrarily defined segments. Later on, Riveiro *et*  
870 *al.* (2011) extended the approach, by accurately representing the arch blocks. Both FEM and LA  
871 models resulted from this study (as shown in Figure 8c). Subsequently, Solla *et al.* (2012) also  
872 accurately represented arches with voussoirs from both SfM photogrammetry and GPR. However, in  
873 this innovating study, the authors defined the internal profiles of the arches from GPR data and  
874 compared various scenarios. A later study also employed GPR for together with orthoimagery to  
875 develop accurate geometric models of arches within the LA to investigate the influence of geometric  
876 uncertainty. In a final study, an array of geometric models was developed, among which with the  
877 image-based approach. Through the specific study, it was shown that whilst 2D block-based models  
878 and 3D continuum-based models showed good agreement for vertical loading, the 3D models (from  
879 mesh-based approach) were advantageous for complex loading cases which include transverse loading  
880 effects.

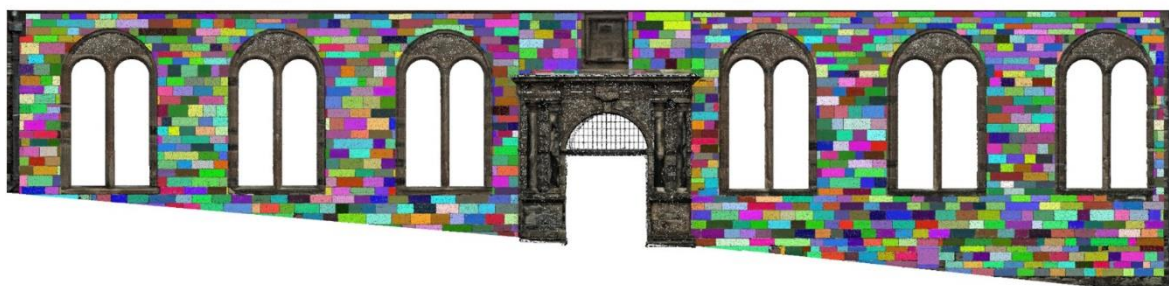
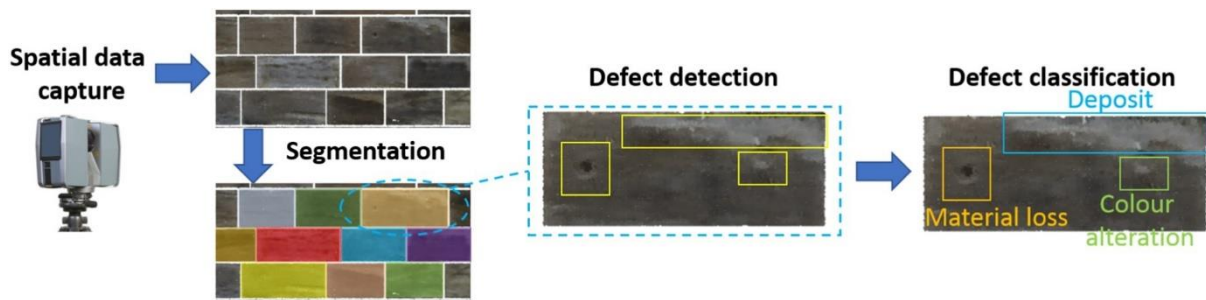
881 Furthermore, apart from masonry bridges, the image-based approach has recently found application  
882 within cultural heritage masonry structures, albeit on a smaller scale. For instance, Napolitano *et al.*  
883 (2019b), developed accurate DEM geometric models of a baptistery from SfM photogrammetry. In a  
884 follow-up study (Napolitano *et al.*, 2019a) the same research team also investigated the importance  
885 of accurate geometry through comparison of simplified and accurate geometric models respectively (as  
886 shown in Figure 8d). The study effectively demonstrated that accurate geometric models were indeed  
887 advantageous for capturing structural behaviour.

888 As can be observed from the aforementioned studies, the main advantage of the image-based approach  
889 is the nature of the geometric data (i.e. orthoimages). Especially in the case such as SfM  
890 photogrammetry, orthoimagery (especially orthomosaics) is more straightforwardly and rapidly  
891 attainable (as demonstrated in Section 5.2.2) in comparison to discrete points whilst it also contains  
892 textural information. However, commonly with the point-based approach, a disadvantage is the  
893 dependency on manual CAD-based block segmentation. It is notable that in an attempt to overcome  
894 this difficulty, various computer vision techniques have been applied for automated-block  
895 segmentation, though not yet explicitly for numerical modelling. Another inherent limitation of image-  
896 based approaches, in general, is also made apparent here which is that they are limited to describing the  
897 structure in two-dimensions since they employ two-dimensional metric information (i.e. of the  
898 orthoimagery) and have a constant, user-assigned thickness in the transverse direction. Although  
899 evidence suggests for the structural analysis of regular masonry structure such as bridges, 2D and 3D  
900 models agree in the absence of transverse loading, two consequences are associated with this limitation:  
901 a) only one layer of masonry is described in the geometric model (i.e. only the spandrel walls and arch  
902 of a masonry arch bridge); and b) the geometric models have planar faces, due to constant transverse  
903 coordinates. Prior to concluding, one final note should be made. Specifically, it should be remembered  
904 that any given numerical model is necessarily a simplification of reality. Therefore, the transition from  
905 the acquired geometry to the numerical model will always involve some elimination of detail. In fact,  
906 keeping an excessively complex geometry may lead to unrealistic or unsafe predictions (e.g., block  
907 shapes that can easily break, excessive roughness of joints). Therefore, there are occasions where the  
908 structural engineer/ numerical modeler should maintain a degree of tolerance (especially for large-scale  
909 structures such as masonry arch bridges). This would eliminate unwanted detail, in order to assure an  
910 efficient structural analysis.

### 911 **6.2.3 The potential of computer vision for automating image-based approaches**

912 Over the last decade, various investigations have demonstrated that computer vision techniques can be  
913 employed for automating the procedure of block segmentation. For instance, (Sithole, 2008) presented  
914 the first development of a deliberate methodology for brick segmentation with point cloud processing

915 techniques. Later on, Willis *et al.* (2010) employed image processing techniques (IPTs) for estimating  
 916 the shape of masonry elements present in the facade of a Gothic building from a single image based on  
 917 automatically detected radiometric variations to separate individual stones the façade of a historic  
 918 masonry church. For masonry/mortar detection, the theoretical background of this method was a  
 919 watershed-based binary with the segmentation of the façade image into stones (black) and mortar  
 920 (white) using a merge criterion based on colour similarity. Later on, Osés *et al.* (2014) also presented  
 921 an IPT-based block segmentation method, based on the detection of mortar lines independent of  
 922 conventional edge detection methods (e.g. Canny, Prewitt etc.). Specifically, to delineate the mortar  
 923 lines, a framework was developed using fine-grained visual categorisation within the open-source  
 924 computer vision library, *OpenCV* by extracting a set of straight-line segments. With a specific focus on  
 925 numerical modelling, however, without structural analysis, Riveiro *et al.* (2016) employed IPTs for  
 926 block segmentation. Block segmentation was based on the intersection of the maximum intensity lines.  
 927 On the other hand, Shen *et al.* (2016) also employed point cloud processing for block segmentation,  
 928 through K-means clustering. Of the first investigations to successfully segment rubble masonry (Valero  
 929 *et al.*, 2018) was based on the 2D continuous wavelet transform with an IPT framework. The same  
 930 research team (Forster *et al.*, 2019) later extended this approach by using machine learning techniques,  
 931 which make it of the most advanced and robust block segmentation methods reviewed, able to extract  
 932 regular masonry or arbitrary shape without a high dependency on block-joint colour contrast such as in  
 933 the case of IPTs. Finally, another recent study (Shen *et al.*, 2019) recently employed IPTs for block  
 934 segmentation, entailing principal component analysis in combination with rectangle fitting.



937 *Figure 9: Automated block segmentation point clouds with machine learning techniques (Forster et al., 2019).*

938 Despite the numerous investigations such as the previous that demonstrate the potential of employing  
939 computer vision for automated block segmentation, no study has yet evaluated the implementation of  
940 automated block segmentation specifically for structural analysis of regular masonry. Therefore,  
941 computer vision techniques have remained unexploited for the high-level numerical modelling of  
942 masonry such as the DEM.

#### 943 **6.2.4 The potential of GPR for defining the internal geometry of the masonry**

944 Prior to concluding this review, it is important to make a note regarding both the aforementioned  
945 structural surveying techniques and approaches to geometric model development. This is that they either  
946 omit or approximate the definition of the internal geometry of the masonry (for example, the cloud-  
947 based approaches only approximate the internal geometry, e.g., with voxels). At the same time, it is  
948 well-known that the internal geometry can highly affect the structural response of a given structure. For  
949 instance, headers of multi-leaf stone masonry wall panels, particularly influence their out-of-plane  
950 behaviour. Additionally, cracks, unconnected wall panels, defects are well known to affect the structural  
951 response of historic masonry buildings. Currently, the experienced contribution of a structural engineer  
952 is still necessary for the manual definition of the internal geometry (e.g., cracks, headers and defects).  
953 Future research should examine a systematic and automated definition of the internal geometry masonry  
954 structure prior to numerical modelling, for example through the employment of GPR, as in Solla *et al.*  
955 (2012).

### 956 **7 Conclusions**

957 This paper presented approaches for the employment non-contact sensing to enhance both the efficiency  
958 and reliability of numerical modelling of historic masonry. It commenced with a review of the high-  
959 level numerical modelling approaches of historic masonry. Then, non-contact sensing techniques for  
960 surveying masonry structures were reviewed, concerning their accuracy and cost-effectivity. These  
961 were: a) the total station; b) the laser tracker; c) Structure-from-Motion (SfM) photogrammetry; and d)  
962 terrestrial laser scanning (TLS). After, approaches of automatically developing geometric models (i.e.,  
963 numerical models prior to structural analysis) from geospatial data were reviewed, concerning their  
964 degree of automation and facility in implementation. These approaches were organized based on the  
965 employment of a: a) point cloud; b) mesh; c) NURBS; d) BIM; e) orthoimage; and f) a sum of discrete  
966 points.

967 Concerning numerical modelling, it was found that an array of numerical modelling approaches has  
968 potential for the high-level structural analysis of masonry structures. However, it was also found that  
969 the majority of the such numerical modelling approaches employ simplified geometric models (i.e. ad-  
970 hoc or idealised/simplified). Consequently, their efficiency is compromised due to the limitations of

971 laborious manual measurements and procedures relating to developing a geometric model. Furthermore,  
972 the fact that the reliability of the geometrical properties is neglected also means that uncertainty is  
973 induced into the structural analysis itself. The reasons for which state-of-the-art numerical modelling  
974 approaches studies neglect the employment of accurate geometric models were attributed to: a)  
975 difficulties in geometric data acquisition; b) the complex geometric model development of the DEM  
976 (i.e. block-by-block); and c) the lack of comprehensive investigation on the effect of geometric  
977 uncertainty to justify the employment of accurate geometric models in the first place.

978 To overcome the difficulty of geometric model development, various non-contact sensing techniques  
979 were reviewed, in their suitability for providing geometric data for numerical modelling rapidly and  
980 reliably. Techniques as SfM photogrammetry were found to be particularly attractive for this, due to its  
981 accuracy (i.e., comparable to TLS), low operational cost and straightforwardly implementation.  
982 Furthermore, concerning the difficulty of geometric model development, various strategies were also  
983 found to greatly improve the efficiency and robustness of the structural analysis. On the one hand, for  
984 continuum-based modelling approaches, the most efficient was considered the cloud-based approach  
985 (e.g., such as through the employment of voxelization). However, it was also highlighted that the only  
986 cloud-based approach found regarded representing the masonry as voxels, i.e., cuboids. It is  
987 recommended that other methods of spatial enumeration should be employed, that better approximate  
988 the anisotropic nature of masonry (for instance with Voronoi blocks, as in (Pulatsu *et al.*, 2019)). On  
989 the other hand, for block-based modelling approaches, the image-based approach, was considered the  
990 most efficient, especially for large-scale masonry structures. However, here it was found that this  
991 approach still relies on manual CAD-based block definition. It is recommended that computer vision  
992 approaches be employed, especially novel technologies such as machine learning (as in (Forster *et al.*,  
993 2019)) for automating this process.

994 Whilst more investigations are necessary on this novel topic, this contribution demonstrates various  
995 approaches for the employment of emerging non-contact sensing techniques to enhance both the  
996 efficiency and robustness of the structural analysis.

## 997 **Acknowledgements**

998 The work presented in this paper has been financially supported by an EPSRC doctoral training award  
999 (case/179/65/82).

## 1000 **References**

1001 Acary, V., Blaise, J., Drap, P., Florenzano, M., Garrec, S. and Jean, M. (1999). NSCD method  
1002 applied to mechanical simulation of masonry in historical buildings using MOMA.

- 1003 *International Symposium WG3 on Simple methods for architectural photogrammetry*. Olinda,  
1004 Brazil, Oct 1999. pp. 225-237
- 1005 Addressi, D. and Sacco, E. (2016). Nonlinear analysis of masonry panels using a kinematic  
1006 enriched plane state formulation. *International Journal of Solids and Structures*, 90, pp. 194-  
1007 214. Doi: 10.1016/j.ijsolstr.2016.03.002
- 1008 Ademovic, N. and Hadzima-Nyarko, M. (2019). Different possibilities for modelling cracked  
1009 masonry structures. *Advanced Technologies, Systems, and Applications III*. Sarajevo, Bosnia  
1010 and Herzegovina, June 20–23, 2019. Springer International Publishing, pp. 113-120
- 1011 Aguilar, F., Agüera, F., M.A, A. and Carvajal, F. (2005). Effects of terrain morphology,  
1012 sampling density, and interpolation methods on grid dem accuracy. *Photogrammetric*  
1013 *Engineering and Remote Sensing*, 71, pp. 805-816. Doi: 10.14358/PERS.71.7.805
- 1014 Ali, S.S. and Page, A.W. (1988). Finite-element model for masonry subjected to concentrated  
1015 loads. *Journal of Structural Engineering-Asce*, 114(8), pp. 1761-1784. Doi:  
1016 10.1061/(ASCE)0733-9445(1988)114:8(1761)
- 1017 Almac, U., Pekmezci, I.P. and Ahunbay, M.G. (2016). Numerical analysis of historic structural  
1018 elements using 3d point cloud data. *The Open Construction and Building Technology Journal*,  
1019 10(Suppl 2: M5), pp. 233-245. Doi: 10.2174/1874836801610010233
- 1020 Altuntas, C., Pehlivanlı, M.E. and Kurban, S. (2017). Low-cost 3D imaging and measurement  
1021 techniques for documentation of Meram masonry arch bridge in Turkey. *International Journal*  
1022 *of Sensors and Sensor Networks Journal of Sensors and Sensor Networks*, 5, pp. 63-69. Doi:  
1023 10.11648/j.ijssn.20170505.11
- 1024 Andriasyan, M., Moyano, J., Nieto-Julián, J.E. and Antón, D. (2020). From point cloud data to  
1025 Building Information Modelling: An automatic parametric workflow for heritage. *Remote*  
1026 *Sensing*, 12(7) Doi: 10.3390/rs12071094
- 1027 Anthoine, A. (1995). Derivation of the in-plane elastic characteristics of masonry through  
1028 homogenization theory. *International Journal of Solids and Structures*, 32(2), pp. 137-163.  
1029 Doi: 10.1016/0020-7683(94)00140-R
- 1030 Arias, P., Armesto, J., Di-Capua, D., Gonzalez-Drigo, R., Lorenzo, H. and Perez-Gracia, V.  
1031 (2007). Digital photogrammetry, GPR and computational analysis of structural damages in a  
1032 mediaeval bridge. *Engineering Failure Analysis*, 14(8), pp. 1444-1457. Doi:  
1033 10.1016/j.engfailanal.2007.02.001
- 1034 Asteris, P., Sarhosis, V., Mohebkhah, A., Plevris, V., Papaloizou, L., Komodromos, P. and  
1035 Lemos, J. (2015). Numerical modeling of historic masonry structures, in: Panagiotis G. Asteris,  
1036 V.P. (ed.) *Handbook of Research on Seismic Assessment and Rehabilitation of Historic*  
1037 *Structures*. 1st edn., pp. 213-256.
- 1038 Baggio, C. and Trovalusci, P. (1998). Limit analysis for no-tension and frictional three-  
1039 dimensional discrete systems. *Mechanics of Structures and Machines*, 26(3), pp. 287-304. Doi:  
1040 10.1080/08905459708945496

- 1041 Baggio, C. and Trovalusci, P. (2000). Collapse behaviour of three-dimensional brick-block  
1042 systems using non-linear programming. *Structural Engineering and Mechanics*, 10, pp. 181-  
1043 195. Doi: 10.12989/sem.2000.10.2.181
- 1044 Bagnolo, V. and Argiolas, R. (2021) 'Scan-to-BIM Process Versus 3D Procedural Modelling of  
1045 Gothic Masonry Vaults' *Springer Tracts in Civil Engineering* [Book Chapter]. pp. 17-31.  
1046 Available at: [https://www.scopus.com/inward/record.uri?eid=2-s2.0-  
1047 85088445847&doi=10.1007%2f978-3-030-49278-  
1048 6\\_2&partnerID=40&md5=51fb07503b13ce8cbabb419901c623a2](https://www.scopus.com/inward/record.uri?eid=2-s2.0-85088445847&doi=10.1007%2f978-3-030-49278-6_2&partnerID=40&md5=51fb07503b13ce8cbabb419901c623a2).
- 1049 Baltsavias, E.P. (1999). Airborne laser scanning: basic relations and formulas. *ISPRS Journal*  
1050 *of Photogrammetry and Remote Sensing*, 54(2-3), pp. 199-214. Doi: 10.1016/S0924-  
1051 2716(99)00015-5
- 1052 Baraldi, D., Reccia, E. and Cecchi, A. (2017). In plane loaded masonry walls: DEM and  
1053 FEM/DEM models. A critical review. *Meccanica*, pp. 1-16. Doi: 10.1007/s11012-017-0704-3
- 1054 Barazzetti, L., Banfi, F., Brumana, R., Gusmeroli, G., Previtali, M. and Schiantarelli, G.  
1055 (2015a). Cloud-to-BIM-to-FEM: Structural simulation with accurate historic BIM from laser  
1056 scans. *Simulation Modelling Practice and Theory*, 57, pp. 71-87. Doi:  
1057 10.1016/j.simpat.2015.06.004
- 1058 Barazzetti, L., Giussani, A., Previtali, M. and Roncoroni, F. (2015b). Laser tracker technology  
1059 for static monitoring of civil infrastructure. *Lasers in Engineering*, 32(3-4), pp. 263-294.  
1060 Available at: [https://www.scopus.com/inward/record.uri?eid=2-s2.0-  
1061 84941626306&partnerID=40&md5=b1a5d0815dd13bb5615f49d7bf8c8b03](https://www.scopus.com/inward/record.uri?eid=2-s2.0-84941626306&partnerID=40&md5=b1a5d0815dd13bb5615f49d7bf8c8b03) [Accessed 13th  
1062 July 2019]
- 1063 Barrile, V., Bilotta, G., Lamari, D. and Meduri, G. (2015). Comparison between techniques for  
1064 generating 3D models of cultural heritage. *Recent Advances in Mechanics, Mechatronics and*  
1065 *Civil, Chemical and Industrial Engineering*. Zakynthos Island, Greece, July 16-20, 2015.  
1066 Proceedings of the 2015 International Conference on Civil Engineering (CIVILENG 2015),  
1067 pp. 140-145
- 1068 Barrile, V., Bilotta, G., Meduri, G., Trovato, S. and D'Amore, E. (2016). Structural modeling  
1069 of a historic castle using close range photogrammetry. *International Journal of Mathematics*  
1070 *and Computers in Simulation*, 10, pp. 370-380. Available at:  
1071 <https://pdfs.semanticscholar.org/8ec1/34a69f0639928f51b0d71160983c17454349.pdf>  
1072 [Accessed 11th February 2020]
- 1073 Barrile, V., Bilotta, G. and Nunnari, A. (2017). UAV and computer vision, detection of  
1074 infrastructure losses and 3D modeling. *ISPRS Annals of Photogrammetry, Remote Sensing and*  
1075 *Spatial Information Sciences*. Safranbolu, Karabuk, Turkey, 11/13. pp. 135-139
- 1076 Bassier, M., Hardy, G., Bejarano-Urrego, L., Drougkas, A., Verstrynge, E., Van Balen, K. and  
1077 Vergauwen, M. (2018). Semi-automated creation of accurate FE meshes of heritage masonry  
1078 walls from point cloud data. *Structural Analysis of Historical Constructions*. Cusco, Peru,  
1079 2018. Springer International Publishing, pp. 305-314

- 1080 Bassier, M. and Vergauwen, M. (2020). Unsupervised reconstruction of Building Information  
1081 Modeling wall objects from point cloud data. *Automation in Construction*, 120 Doi:  
1082 10.1016/j.autcon.2020.103338
- 1083 Beatini, V., Royer-Carfagni, G. and Tasora, A. (2019). A non-smooth-contact-dynamics  
1084 analysis of Brunelleschi's cupola: an octagonal vault or a circular dome? *Meccanica*, 54(3), pp.  
1085 525-547. Doi: 10.1007/s11012-018-00934-9
- 1086 Berto, L., Saetta, A., Scotta, R. and Vitaliani, R. (2002). An orthotropic damage model for  
1087 masonry structures. *International Journal for Numerical Methods in Engineering*, 55(2), pp.  
1088 127-157. Doi: 10.1002/nme.495
- 1089 Binda, L., Cardani, G. and Saisi, A. (2009). A classification of structures and masonries for the  
1090 adequate choice of repair, in: Groot, C. (ed.) *Workshop Repair Mortars for Historic Masonry*.  
1091 1st edn. Delft University of Technology, the Netherlands, pp. 20-34.
- 1092 Bitelli, G., Castellazzi, G., D'Altri, A., Miranda, S., Lambertini, A. and Selvaggi, I. (2016).  
1093 Automated voxel model from point clouds for structural analysis of cultural heritage. *ISPRS*  
1094 *XXI - International Archives of the Photogrammetry, Remote Sensing and Spatial Information*  
1095 *Sciences*. Prague, Czech republic, 06/16. pp. 191-197
- 1096 Bobet, A., Fakhimi, A., Johnson, S., Morris, J., Tonon, F. and Yeung, M. (2009). Numerical  
1097 models in discontinuous media: Review of advances for rock mechanics applications. *Journal*  
1098 *of Geotechnical and Geoenvironmental Engineering*, 135, pp. 1547-1561. Doi:  
1099 10.1061/(ASCE)GT.1943-5606.0000133
- 1100 Bosché, F., Forster, A. and Valero, E. (2015) *3D surveying technologies and applications: Point*  
1101 *clouds and beyond*. Heriot-Watt University. [Online]. Available at:  
1102 <https://pureapps2.hw.ac.uk/ws/portalfiles/portal/9482712/report.pdf> [Accessed 19th January  
1103 2020]
- 1104 Brenner, C. (2005). Building reconstruction from images and laser scanning. *International*  
1105 *Journal of Applied Earth Observation and Geoinformation*, 6(3), pp. 187-198. Doi:  
1106 10.1016/j.jag.2004.10.006
- 1107 Bruno, N., Coisson, E., Diotri, F., Ferrari, L., Mikolajewska, S., Morra di Cella, U., Roncella,  
1108 R. and Zerbi, A. (2019). History, geometry, structure: Interdisciplinary analysis of a historical  
1109 bridge. *ISPRS - International Archives of the Photogrammetry, Remote Sensing and Spatial*  
1110 *Information Sciences*, XLII-2/W11, pp. 317-323. Doi: 10.5194/isprs-archives-XLII-2-W11-  
1111 317-2019
- 1112 Bui, T.T., Limam, A., Sarhosis, V. and Hjiij, M. (2017). Discrete element modelling of the in-  
1113 plane and out-of-plane behaviour of dry-joint masonry wall constructions. *Engineering*  
1114 *Structures*, 136, pp. 277-294. Doi: 10.1016/j.engstruct.2017.01.020
- 1115 Castellazzi, G., Altri, M.A., Bitelli, G., Selvaggi, I. and Lambertini, A. (2015). From laser  
1116 scanning to finite element analysis of complex buildings by using a semi-automatic procedure.  
1117 *Sensors*, 15(8), pp. 18360–18380. Doi: 10.3390/s150818360

- 1118 Castellazzi, G., D'Altri, A.M., de Miranda, S. and Ubertini, F. (2017). An innovative numerical  
1119 modeling strategy for the structural analysis of historical monumental buildings. *Engineering*  
1120 *Structures*, 132, pp. 229-248. Doi: 10.1016/j.engstruct.2016.11.032
- 1121 Cavalagli, N., Cluni, F. and Gusella, V. (2013). Evaluation of a Statistically Equivalent Periodic  
1122 Unit Cell for a quasi-periodic masonry. *International Journal of Solids and Structures*, 50(25),  
1123 pp. 4226-4240. Doi: 10.1016/j.ijsolstr.2013.08.027
- 1124 Cavicchi, A. and Gambarotta, L. (2006). Two-dimensional finite element upper bound limit  
1125 analysis of masonry bridges. *Computers & Structures*, 84(31), pp. 2316-2328. Doi:  
1126 10.1016/j.compstruc.2006.08.048
- 1127 Cecchi, A. and Milani, G. (2008). A kinematic FE limit analysis model for thick English bond  
1128 masonry walls. *International Journal of Solids and Structures*, 45(5), pp. 1302-1331. Doi:  
1129 10.1016/j.ijsolstr.2007.09.019
- 1130 Cecchi, A., Milani, G. and Tralli, A. (2007). A Reissner–Mindlin limit analysis model for out-  
1131 of-plane loaded running bond masonry walls. *International Journal of Solids and Structures*,  
1132 44(5), pp. 1438-1460. Doi: 10.1016/j.ijsolstr.2006.06.033
- 1133 Chen, S. (2012). Laser scanning technology for bridge monitoring, in: *Laser Scanner*  
1134 *Technology*.
- 1135 Chen, S., Laefer, D., Mangina, E., Zolanvari, I. and Byrne, J. (2019). UAV bridge inspection  
1136 through evaluated 3D reconstructions. *Journal of Bridge Engineering*, 24, p. 05019001. Doi:  
1137 10.1061/(ASCE)BE.1943-5592.0001343
- 1138 Chetouane, B., Dubois, F., Vinches, M. and Bohatier, C. (2005). NSCD discrete element  
1139 method for modelling masonry structures. *International Journal for Numerical Methods in*  
1140 *Engineering*, 64(1), pp. 65-94. Available at: [Go to ISI://WOS:000231641100004](https://doi.org/10.1016/j.ijsolstr.2005.01.004) [Accessed  
1141 11th February 2020]
- 1142 Chisari, C., Macorini, L., Amadio, C. and Izzuddin, B. (2018). Identification of mesoscale  
1143 model parameters for brick-masonry. *International Journal of Solids and Structures*, 146, pp.  
1144 224-240. Doi: 10.1016/j.ijsolstr.2018.04.003
- 1145 Como, M. (2013) *Statics of Historic Masonry Constructions*. 1st edn. Springer Berlin  
1146 Heidelberg.
- 1147 Conde, B., F. Ramos, L., Oliveira, D., Riveiro, B. and Solla, M. (2017). Structural assessment  
1148 of masonry arch bridges by combination of non-destructive testing techniques and three-  
1149 dimensional numerical modelling: Application to Vilanova bridge. *Engineering Structures*,  
1150 148, pp. 621-638. Doi: 10.1016/j.engstruct.2017.07.011
- 1151 Cundall, P.A. (1971). A computer model for simulating progressive, large - scale movement in  
1152 blocky rock systems. *Proceedings of the Symposium of the International Society of Rock*  
1153 *Mechanics*. Nancy, France, 1971. pp. 129-136
- 1154 Cundall, P.A. and Hart, R.D. (1992). Numerical modelling of discontinua. *Engineering*  
1155 *Computations*, 9(2), pp. 101-113. Doi: 10.1108/eb023851

- 1156 Cundall, P.A. and Strack, O.D.L. (1980). A discrete numerical-model for granular assemblies -  
 1157 reply. *Geotechnique*, 30(3), pp. 335-336. Available at: [<Go to](#)  
 1158 [ISI>://WOS:A1980KM60500017](#) [Accessed 11th February 2020]
- 1159 D'Altri, A.M., de Miranda, S., Castellazzi, G. and Sarhosis, V. (2018a). A 3D detailed micro-  
 1160 model for the in-plane and out-of-plane numerical analysis of masonry panels. *Computers &*  
 1161 *Structures*, 206, pp. 18-30. Doi: 10.1016/j.compstruc.2018.06.007
- 1162 D'Altri, A.M., Messali, F., Rots, J., Castellazzi, G. and de Miranda, S. (2019). A damaging  
 1163 block-based model for the analysis of the cyclic behaviour of full-scale masonry structures.  
 1164 *Engineering Fracture Mechanics*, 209, pp. 423-448. Doi: 10.1016/j.engfracmech.2018.11.046
- 1165 D'Altri, A.M., Milani, G., Miranda, S., Castellazzi, G. and Sarhosis, V. (2018b). Stability  
 1166 analysis of leaning historic masonry structures. *Automation in Construction*, 92, pp. 199–213.  
 1167 Doi: 10.1016/j.autcon.2018.04.003
- 1168 D'Altri, A.M., Castellazzi, G. and de Miranda, S. (2018). Collapse investigation of the Arquata  
 1169 del Tronto medieval fortress after the 2016 Central Italy seismic sequence. *Journal of Building*  
 1170 *Engineering*, 18, pp. 245-251. Doi: <https://doi.org/10.1016/j.jobbe.2018.03.021>
- 1171 D'Altri, A.M., Sarhosis, V., Milani, G., Rots, J., Cattari, S., Lagomarsino, S., Sacco, E., Tralli,  
 1172 A., Castellazzi, G. and de Miranda, S. (2019). Modeling strategies for the computational  
 1173 analysis of unreinforced masonry structures: Review and classification. *Archives of*  
 1174 *Computational Methods in Engineering*, pp. 1-33. Doi: 10.1007/s11831-019-09351-x
- 1175 Dai, F. and Lu, M. (2010). Assessing the accuracy of applying photogrammetry to take  
 1176 geometric measurements on building products *Journal of Construction Engineering and*  
 1177 *Management*, 136(2), pp. 242-250. Doi: 10.1061/(ASCE)CO.1943-7862.0000114
- 1178 Del Piero, G. (1989). Constitutive equation and compatibility of the external loads for linear  
 1179 elastic masonry-like materials. *Meccanica*, 24(3), pp. 150-162. Doi: 10.1007/BF01559418
- 1180 Dialer, C. (1992). A distinct element approach for the deformation behaviour of shear stressed  
 1181 masonry panels. *Proceedings of the 6th Canadian masonry symposium*. Saskatchewan,  
 1182 Canada, 15-17 June. pp. 765-776
- 1183 Dietrich, J. (2016). Riverscape mapping with helicopter-based structure-from-motion  
 1184 photogrammetry. *Geomorphology*, 252, pp. 144–157. Doi: 10.1016/j.geomorph.2015.05.008
- 1185 Dubois, F. and Jean, M. (2003). LMGC90 une plateforme de développement dédiée à la  
 1186 modélisation des problèmes d'interaction. *Actes du Sixieme Colloque National en Calcul des*  
 1187 *Structures*. France, france. pp. 111-118
- 1188 Eltner, A., Kaiser, A., Castillo, C., Rock, G., Neugirg, F. and Abellan, A. (2016). Image-based  
 1189 surface reconstruction in geomorphometry - merits, limits and developments. *Earth Surface*  
 1190 *Dynamics*, 4, pp. 359-389. Doi: 10.5194/esurf-4-359-2016
- 1191 Estler, W.T., Edmundson, K.L., Peggs, G.N. and Parker, D.H. (2002). Large-scale metrology -  
 1192 An update. *CIRP Annals - Manufacturing Technology*, 51(2), pp. 587-609. Doi:  
 1193 10.1016/S0007-8506(07)61702-8

- 1194 Ferris, M.C. and Tin-Loi, F. (2001). Limit analysis of frictional block assemblies as a  
1195 mathematical program with complementarity constraints. *International Journal of Mechanical*  
1196 *Sciences*, 43(1), pp. 209-224. Doi: 10.1016/S0020-7403(99)00111-3
- 1197 Fishwick, R.J. (1996) *Limit analysis of rigid block structures*. Ph.D. thesis. University of  
1198 Portsmouth [Online]. Available at: <https://ethos.bl.uk/OrderDetails.do?uin=uk.bl.ethos.310412>  
1199 [Accessed 5th December 2019]
- 1200 Forgács, T., Rendes, S., Ádány, S. and Sarhosis, V. (2019). Mechanical role of spandrel walls  
1201 on the capacity of masonry arch bridges. *9th International Conference on Arch Bridges*. Cham,  
1202 Switzerland, 2-4 October 2019. Springer International Publishing, pp. 221-229
- 1203 Forgacs, T., Sarhosis, V. and Bagi, K. (2017). Minimum thickness of semi-circular skewed  
1204 masonry arches. *Engineering Structures*, 140, pp. 317-336. Doi:  
1205 10.1016/j.engstruct.2017.02.036
- 1206 Forgács, T., Sarhosis, V. and Bagi, K. (2018). Influence of construction method on the load  
1207 bearing capacity of skew masonry arches. *Engineering Structures*, 168, pp. 612-627. Doi:  
1208 10.1016/j.engstruct.2018.05.005
- 1209 Forster, A., Valero, E. and Bosché, F. (2019). Automated defect detection and classification in  
1210 ashlar masonry walls using machine learning. *Automation in Construction*, 106, p. 102846.  
1211 Doi: 10.1016/j.autcon.2019.102846
- 1212 Gambarotta, L. and Lagomarsino, S. (1997). Damage models for the seismic response of brick  
1213 masonry shear walls. Part I: The mortar joint model and its applications. *Earthquake*  
1214 *Engineering & Structural Dynamics*, 26, pp. 423-439. Doi: 10.1002/(SICI)1096-  
1215 9845(199704)26:4<423::AID-EQE650>3.0.CO;2-#
- 1216 Garrity, S.W. (2013). Strengthening of Masonry Arch Bridges with Near-Surface  
1217 Reinforcement: A Case Study. *International Journal of Engineering and Technology*, 5, pp.  
1218 370-373. Doi: 10.7763/IJET.2013.V5.577
- 1219 Godio, M., Stefanou, I. and Sab, K. (2018). Effects of the dilatancy of joints and of the size of  
1220 the building blocks on the mechanical behavior of masonry structures. *Meccanica*, 53(7), pp.  
1221 1629-1643. Doi: 10.1007/s11012-017-0688-z
- 1222 Godio, M., Stefanou, I., Sab, K., Sulem, J. and Sakji, S. (2017). A limit analysis approach based  
1223 on Cosserat continuum for the evaluation of the in-plane strength of discrete media: Application  
1224 to masonry. *European Journal of Mechanics - A/Solids*, 66, pp. 168-192. Doi:  
1225 10.1016/j.euromechsol.2017.06.011
- 1226 Golparvar-Fard, M., Bohn, J., Teizer, J., Savarese, S. and Peña-Mora, F. (2011). Evaluation of  
1227 image-based modeling and laser scanning accuracy for emerging automated performance  
1228 monitoring techniques. *Automation in Construction*, 20(8), pp. 1143-1155. Doi:  
1229 10.1016/j.autcon.2011.04.016
- 1230 Haala, N. and Rothermel, M. (2012). Dense multi-stereo matching for high quality digital  
1231 elevation models. *Photogrammetrie - Fernerkundung - Geoinformation*, 2012, pp. 331-343.  
1232 Doi: 10.1127/1432-8364/2012/0121

- 1233 Haciefendioğlu, K. and Maraş, E.E. (2016). Photogrammetry in documentation and ambient  
1234 vibration test of historical masonry minarets. *Experimental Techniques*, 40(6), pp. 1527-1537.  
1235 Doi: 10.1007/s40799-016-0137-2
- 1236 Harwin, S., Lucieer, A. and Osborn, J. (2015). The impact of the calibration method on the  
1237 accuracy of point clouds derived using unmanned aerial vehicle multi-view stereopsis. *Remote*  
1238 *Sensing*, 7, pp. 11933-11953. Doi: 10.3390/rs70911933
- 1239 Hendry, E. (2001). Masonry walls: materials and construction. *Construction and Building*  
1240 *Materials*, 15, pp. 323-330. Doi: 10.1016/S0950-0618(01)00019-8
- 1241 Heyman, J. (1969). The safety of masonry arches. *International Journal of Mechanical*  
1242 *Sciences*, 11(4), pp. 363-385. Doi: 10.1016/0020-7403(69)90070-8
- 1243 Heyman, J. (1997) *The stone skeleton: Structural engineering of masonry architecture*. 2nd  
1244 (reprint edition) edn. Cambridge University Press.
- 1245 Highway Agency (2001). *Highway structures: Inspection and maintenance. Assessment.*  
1246 *Assessment of highway bridges and structures (BA 16/97)*. London: HMSO. [Online]. Available  
1247 at: <https://www.thenbs.com/PublicationIndex/documents/details?Pub=HA&DocID=254890>  
1248 [Accessed 11th November 2019]
- 1249 Hinks, T. (2011) *Geometric processing techniques for urban aerial laser scan data*. Ph.D.  
1250 thesis. University College Dublin [Online]. Available at:  
1251 <https://tommyhinks.files.wordpress.com/2012/02/thinks-thesis-single.pdf> [Accessed 5th  
1252 December 2019]
- 1253 Hinks, T., Carr, H., Linh, T.H. and Laefer, D.F. (2012). Point cloud data conversion into solid  
1254 models via point-based voxelization. *Journal of Surveying Engineering*, 139(2), pp. 72-83.  
1255 Doi: 10.1061/(Asce)Su.1943-5428.0000097
- 1256 Historic England (2017) *Photogrammetric applications for cultural heritage. Guidance for*  
1257 *good practise*. 1st edn. Swindon. Historic England.
- 1258 Hofstetter, G., Feist, C., Lehar, H., Theiner, Y., Valentini, B. and Winkler, B. (2011). Plasticity  
1259 based crack models and applications, in: Hofstetter, G. and Meschke, G. (eds.) *Numerical*  
1260 *Modeling of Concrete Cracking*. Vienna: Springer Vienna, pp. 161-219.
- 1261 Iman Zolanvari, S.M. and Laefer, D.F. (2016). Slicing method for curved façade and window  
1262 extraction from point clouds. *ISPRS Journal of Photogrammetry and Remote Sensing*, 119, pp.  
1263 334-346. Doi: 10.1016/j.isprsjprs.2016.06.011
- 1264 Itasca (2019a) *ITASCA. 3DEC 5.2 – Universal distinct element code manual. Theory and*  
1265 *background*. Mineapolis. [Computer program]. Available at: [www.itasca.com](http://www.itasca.com) [Accessed 19th  
1266 January 2020]
- 1267 Itasca (2019b) *ITASCA. PFC – Particle flow code manual. Theory and background*. Mineapolis.  
1268 [Computer program]. Available at: [www.itasca.com](http://www.itasca.com) [Accessed 19th January 2020]

- 1269 Itasca (2019c) *ITASCA. UDEC – Universal distinct element code manual. Theory and*  
 1270 *background. Minneapolis.* [Computer program]. Available at: [www.itasca.com](http://www.itasca.com) [Accessed 19th  
 1271 January 2020]
- 1272 James, M. and Robson, S. (2012). Straightforward reconstruction of 3D surfaces and  
 1273 topography with a camera: Accuracy and geoscience application. *Journal of Geophysical*  
 1274 *Research*, 117, p. F03017. Doi: 10.1029/2011JF002289
- 1275 James, M.R., Robson, S., d'Oleire-Oltmanns, S. and Niethammer, U. (2017). Optimising UAV  
 1276 topographic surveys processed with structure-from-motion: Ground control quality, quantity  
 1277 and bundle adjustment. *Geomorphology*, 280, pp. 51-66. Doi:  
 1278 10.1016/j.geomorph.2016.11.021
- 1279 Jiang, K. and Esaki, T. (2002). Quantitative evaluation of stability changes in historical stone  
 1280 bridges in Kagoshima, Japan, by weathering. *Engineering Geology*, 63, pp. 83-91. Doi:  
 1281 10.1016/S0013-7952(01)00071-0
- 1282 Jirásek, M. (2011). Damage and smeared crack models, in: Hofstetter, G. and Meschke, G.  
 1283 (eds.) *Numerical Modeling of Concrete Cracking*. Vienna: Springer Vienna, pp. 1-49.
- 1284 Kassotakis, N., Sarhosis, V., Peppas, M.V. and Mills, J. (2020). Quantifying the effect of  
 1285 geometric uncertainty on the structural behaviour of arches developed from tape measurement  
 1286 and Structure-from-Motion (SfM) photogrammetry. *Engineering Structures*, - Doi: Accepted  
 1287 17th December 2020
- 1288 Kim, M.K., Wang, Q. and Li, H. (2019). Non-contact sensing based geometric quality  
 1289 assessment of buildings and civil structures: A review. *Automation in Construction*, 100, pp.  
 1290 163-179. Doi: 10.1016/j.autcon.2019.01.002
- 1291 Korumaz, M., Betti, M., Conti, A., Tucci, G., Bartoli, G., Bonora, V., Korumaz, A.G. and  
 1292 Fiorini, L. (2017). An integrated Terrestrial Laser Scanner (TLS), Deviation Analysis (DA) and  
 1293 Finite Element (FE) approach for health assessment of historical structures. A minaret case  
 1294 study. *Engineering Structures*, 153, pp. 224-238. Doi: 10.1016/j.engstruct.2017.10.026
- 1295 Lemos, J. (1995). Assessment of the ultimate load of a masonry arch using discrete elements,  
 1296 in: *Journal of Computer Methods in Structural Masonry*. Swansea, UK: Books and Journals  
 1297 International, pp. 294-302.
- 1298 Lemos, J.V. (2007). Discrete element modeling of masonry structures. *International Journal*  
 1299 *of Architectural Heritage*, 1(2), pp. 190-213. Doi: 10.1080/15583050601176868
- 1300 Leonetti, L., Greco, F., Trovalusci, P., Luciano, R. and Masiani, R. (2018). A multiscale damage  
 1301 analysis of periodic composites using a couple-stress/Cauchy multidomain model: Application  
 1302 to masonry structures. *Composites Part B: Engineering*, 141, pp. 50-59. Doi:  
 1303 10.1016/j.compositesb.2017.12.025
- 1304 LimitState (2019) *Ring ® Version 3.0* [Computer program]. Available at:  
 1305 <http://limitstate.com/ring> [Accessed 19th January 2020]

- 1306 Linh, T.H. and Laefer, D.F. (2013). Validating computational models from laser scanning data  
 1307 for historic facades. *Journal of Testing and Evaluation*, 41(3), pp. 481-496. Doi:  
 1308 10.1520/Jte20120243
- 1309 Linh, T.H. and Laefer, D.F. (2014). Octree-based, automatic building facade generation from  
 1310 LiDAR data. *Computer-Aided Design*, 53, pp. 46-61. Doi: 10.1016/j.cad.2014.03.001
- 1311 Linh, T.H., Laefer, D.F., Hinks, T. and Carr, H. (2012). Flying voxel method with delaunay  
 1312 triangulation criterion for facade/feature detection for computation. *Journal of Computing in*  
 1313 *Civil Engineering*, 26(6), pp. 691-707. Doi: 10.1061/(Asce)Cp.1943-5487.0000188
- 1314 Liu, S.G., Li, Z.J., Zhang, H., Wu, W., Zhong, G.H. and Lou, S. (2018). A 3-D DDA damage  
 1315 analysis of brick masonry buildings under the impact of boulders in mountainous areas. *Journal*  
 1316 *of Mountain Science*, 15(3), pp. 657-671. Doi: 10.1007/s11629-017-4453-5
- 1317 Livesley, R.K. (1978). Limit analysis of structures formed from rigid blocks. *International*  
 1318 *Journal for Numerical Methods in Engineering*, 12(12), pp. 1853-1871. Doi:  
 1319 10.1002/nme.1620121207
- 1320 Lopez, J., Oller, S., Oñate, E. and Lubliner, J. (1999). A homogeneous constitutive model for  
 1321 masonry. *International Journal for Numerical Methods in Engineering*, 46(10), pp. 1651-1671.  
 1322 Doi: 10.1002/(SICI)1097-0207(19991210)46:10<1651::AID-NME718>3.0.CO;2-2
- 1323 Lotfi, H.R. and Shing, P.B. (1991). An appraisal of smeared crack models for masonry shear  
 1324 wall analysis. *Computers & Structures*, 41(3), pp. 413-425. Doi: 10.1016/0045-  
 1325 7949(91)90134-8
- 1326 Lotfi, H.R. and Shing, P.B. (1994). Interface model applied to fracture of masonry structures.  
 1327 *Journal of Structural Engineering*, 120(1), pp. 63-80. Doi: 10.1061/(ASCE)0733-  
 1328 9445(1994)120:1(63)
- 1329 Lourenco, P. (1996) *Computational strategies for masonry structures*. Ph.D. thesis. Delft  
 1330 University of Technology [Online]. Available at:  
 1331 [http://www.hms.civil.uminho.pt/arq/fich/1996\\_PhD\\_PBLourenco.pdf](http://www.hms.civil.uminho.pt/arq/fich/1996_PhD_PBLourenco.pdf) [Accessed 5th  
 1332 December 2019]
- 1333 Lourenco, P. (2002). Computations on historic masonry structures. *Progress in Structural*  
 1334 *Engineering and Materials*, 4, pp. 301-319. Doi: 10.1002/pse.120
- 1335 Lourenco, P.B. and Rots, J.G. (1997). Multisurface interface model for analysis of masonry  
 1336 structures. *Journal of Engineering Mechanics-Asce*, 123(7), pp. 660-668. Doi:  
 1337 10.1061/(ASCE)0733-9399(1997)123:7(660)
- 1338 Lowe, D.G. (2004). Distinctive image features from scale-invariant keypoints. *International*  
 1339 *Journal of Computer Vision*, 60(2), pp. 91-110. Doi: 10.1023/B:VISI.0000029664.99615.94
- 1340 Lubowiecka, I., Arias, P., Riveiro, B. and Solla, M. (2011). Multidisciplinary approach to the  
 1341 assessment of historic structures based on the case of a masonry bridge in Galicia (Spain).  
 1342 *Computers & Structures*, 89, pp. 1615-1627. Doi: 10.1016/j.compstruc.2011.04.016

- 1343 Macorini, L. and Izzuddin, B.A. (2011). A non-linear interface element for 3D mesoscale  
1344 analysis of brick-masonry structures. *International Journal for Numerical Methods in*  
1345 *Engineering*, 85(12), pp. 1584-1608. Doi: 10.1002/nme.3046
- 1346 Meschini, A., Leoni, G., Petrucci, E., Sicuranza, F., Zona, A., Piattoni, Q., Dezi, L. and  
1347 Dall'Asta, A. (2015). An integrated Survey Experience for Assessing the Seismic Vulnerability  
1348 of Senigallia's Fortress (Italy): Documentation for Conservation and FEM Modeling. *Digital*  
1349 *Heritage 2015*. Granada, Spain, 28 Sept.-2 Oct. 2015. pp. 21-28
- 1350 Milani, G. (2008). 3D upper bound limit analysis of multi-leaf masonry walls. *International*  
1351 *Journal of Mechanical Sciences*, 50(4), pp. 817-836. Doi: 10.1016/j.ijmecsci.2007.11.003
- 1352 Milani, G. (2011). Simple lower bound limit analysis homogenization model for in- and out-  
1353 of-plane loaded masonry walls. *Construction and Building Materials*, 25(12), pp. 4426-4443.  
1354 Doi: 10.1016/j.conbuildmat.2011.01.012
- 1355 Milani, G., Beyer, K. and Dazio, A. (2009). Upper bound limit analysis of meso-mechanical  
1356 spandrel models for the pushover analysis of 2D masonry frames. *Engineering Structures*,  
1357 31(11), pp. 2696-2710. Doi: 10.1016/j.engstruct.2009.06.015
- 1358 Milani, G., Casolo, S., Naliato, A. and Tralli, A. (2012). Seismic assessment of a medieval  
1359 masonry tower in northern Italy by limit, nonlinear static, and full dynamic analyse.  
1360 *International Journal of Architectural Heritage*, 6(5), pp. 489-524. Doi:  
1361 10.1080/15583058.2011.588987
- 1362 Milani, G., Lourenço, P. and Tralli, A. (2006a). Homogenization approach for the limit analysis  
1363 of out-of-plane loaded masonry walls. *Journal of Structural Engineering*, 132(10), pp. 1650-  
1364 1663. Doi: 10.1061/(ASCE)0733-9445(2006)132:10(1650)
- 1365 Milani, G., Lourenço, P.B. and Tralli, A. (2006b). Homogenised limit analysis of masonry  
1366 walls, Part I: Failure surfaces. *Computers & Structures*, 84(3), pp. 166-180. Doi:  
1367 10.1016/j.compstruc.2005.09.005
- 1368 Mills, J. and Barber, D. (2004). Geomatics techniques for structural surveying. *Journal of*  
1369 *Surveying Engineering*, 57, pp. 56-64 Doi: 10.1061/(ASCE)0733-9453(2004)130:2(56)
- 1370 Moreau, J.J. (1988). Free boundaries and non-smooth solutions to some field-equations -  
1371 variational characterization through the transport method. *Lecture Notes in Control and*  
1372 *Information Sciences*, 100, pp. 235-264. Available at: [Go to ISI://WOS:A1988M644400013](https://www.isinet.com/doi/10.1016/0167-6911(88)90013-9)  
1373 [Accessed 23th April 2020]
- 1374 Morer, P., de Arteaga, I., Armesto, J. and Arias, P. (2011). Comparative structural analyses of  
1375 masonry bridges: An application to the Cernadela Bridge. *Journal of Cultural Heritage*, 12(3),  
1376 pp. 300-309. Doi: 10.1016/j.culher.2011.01.006
- 1377 Morer, P., de Arteaga, I. and Ortueta, A. (2013). A low-cost photogrammetric methodology to  
1378 obtain geometrical data of masonry arch bridges. *Journal of Architectural Conservation*, 19(3),  
1379 pp. 246-264. Doi: 10.1080/13556207.2013.869974

- 1380 Munjiza, A., Owen, D.R.J. and Bicanic, N. (1995). A combined finite-discrete element method  
1381 in transient dynamics of fracturing solids. *Engineering Computations*, 12(2), pp. 145-174. Doi:  
1382 10.1108/02644409510799532
- 1383 Napolitano, R. and Glisic, B. (2019). Understanding the function of bonding courses in  
1384 masonry construction: An investigation with mixed numerical methods. *Journal of Cultural*  
1385 *Heritage*, 39, pp. 120-129. Doi: 10.1016/j.culher.2019.03.007
- 1386 Napolitano, R., Hess, M. and Glisic, B. (2019a). Quantifying the differences in documentation  
1387 and modeling levels for building pathology and diagnostics. *Archives of Computational*  
1388 *Methods in Engineering*, pp. 1-18. Doi: 10.1007/s11831-019-09350-y
- 1389 Napolitano, R.K., Hess, M. and Glisic, B. (2019b). The foundation walls of the baptistry Di  
1390 San Giovanni: A combination of laser scanning and finite-distinct element modeling to  
1391 ascertain damage origins. *International Journal of Architectural Heritage*, 13(7), pp. 1180-  
1392 1193. Doi: 10.1080/15583058.2019.1582726
- 1393 Olsen, M. and Kayen, R. (2012). Post-earthquake and tsunami 3D laser scanning forensic  
1394 investigations. *ASCE Sixth Congress on Forensic Engineering*. San Francisco, June 2012. pp.  
1395 477-486
- 1396 Orduña, A. and Lourenço, P.B. (2005). Three-dimensional limit analysis of rigid blocks  
1397 assemblages. Part I: Torsion failure on frictional interfaces and limit analysis formulation.  
1398 *International Journal of Solids and Structures*, 42(18), pp. 5140-5160. Doi:  
1399 10.1016/j.ijsolstr.2005.02.010
- 1400 Oses, N., Dornaika, F. and Moujahid, A. (2014). Image-based delineation and classification of  
1401 built heritage masonry. *Remote Sensing*, 6(3), pp. 782-789. Doi: 10.3390/rs6031863
- 1402 Owen, R.D., Perić, D., Petrinic, N. and James, J.P. (1998) *Finite/discrete element models for*  
1403 *assessment and repair of masonry structures*. [Online]. Available at: [https://cintec.com/wp-](https://cintec.com/wp-content/uploads/2015/04/Finite_discrete-Elements.pdf)  
1404 [content/uploads/2015/04/Finite\\_discrete-Elements.pdf](https://cintec.com/wp-content/uploads/2015/04/Finite_discrete-Elements.pdf) [Accessed 19th January 2020]
- 1405 Page, A.W. (1978). Finite-element model for masonry. *Journal of the Structural Division-Asce*,  
1406 104(8), pp. 1267-1285. Available at: [Go to ISI://WOS:A1978FK58500007](https://doi.org/10.1061/(ASCE)0005-4021(1978)104:8(1267)) [Accessed 23th  
1407 April 2020]
- 1408 Pelà, L., Cervera, M., Oller, S. and Chiumenti, M. (2014). A localized mapped damage model  
1409 for orthotropic materials. *Engineering Fracture Mechanics*, 124-125, pp. 196-216. Doi:  
1410 10.1016/j.engfracmech.2014.04.027
- 1411 Pelà, L., Cervera, M. and Roca, P. (2011). Continuum damage model for orthotropic materials:  
1412 Application to masonry. *Computer Methods in Applied Mechanics and Engineering*, 200(9),  
1413 pp. 917-930. Doi: 10.1016/j.cma.2010.11.010
- 1414 Pelà, L., Cervera, M. and Roca, P. (2013). An orthotropic damage model for the analysis of  
1415 masonry structures. *Construction and Building Materials*, 41, pp. 957-967. Doi:  
1416 10.1016/j.conbuildmat.2012.07.014

- 1417 Pepe, M., Fregonese, I. and Crocetto, N. (2019). Application of the SfM approach in building  
 1418 3D models of masonry bridges using nadir, oblique and zenith images obtained from UAV  
 1419 aerial platform. *IJCIET*, Volume 10, (3), pp. 1626 - 1638. Available at:  
 1420 [http://d.researchbib.com/f/9nq3q3YzyuMJ1yYzAioF9ALKA0MKWOMT1cov9IpTkiLJETo](http://d.researchbib.com/f/9nq3q3YzyuMJ1yYzAioF9ALKA0MKWOMT1cov9IpTkiLJETo2kxMKViFHcQFHIHKmRjKmNmKmR2ZF9WFxAWEIEsZGOsZQAsZGLkYaOxMt.pdf)  
 1421 [2kxMKViFHcQFHIHKmRjKmNmKmR2ZF9WFxAWEIEsZGOsZQAsZGLkYaOxMt.pdf](http://d.researchbib.com/f/9nq3q3YzyuMJ1yYzAioF9ALKA0MKWOMT1cov9IpTkiLJETo2kxMKViFHcQFHIHKmRjKmNmKmR2ZF9WFxAWEIEsZGOsZQAsZGLkYaOxMt.pdf)  
 1422 [Accessed 23th April 2020]
- 1423 Peppas, M.V. (2018) *Morphology-based landslide monitoring with an unmanned aerial vehicle*.  
 1424 Ph.D. thesis. University of Newcastle [Accessed 5th December 2019]
- 1425 Perez-Aparicio, J.L., Bravo, R. and Ortiz, P. (2013). Refined element discontinuous numerical  
 1426 analysis of dry-contact masonry arches. *Engineering Structures*, 48, pp. 578-587. Doi:  
 1427 10.1016/j.engstruct.2012.09.027
- 1428 Petracca, M., Pelà, L., Rossi, R., Zaghi, S., Camata, G. and Spacone, E. (2017). Micro-scale  
 1429 continuous and discrete numerical models for nonlinear analysis of masonry shear walls.  
 1430 *Construction and Building Materials*, 149, pp. 296–314. Doi:  
 1431 10.1016/j.conbuildmat.2017.05.130
- 1432 Pieraccini, M., Dei, D., Betti, M., Bartoli, G., Tucci, G. and Guardini, N. (2014). Dynamic  
 1433 identification of historic masonry towers through an expeditious and no-contact approach:  
 1434 Application to the “Torre del Mangia” in Siena (Italy). *Journal of Cultural Heritage*, 15(3), pp.  
 1435 275-282. Doi: 10.1016/j.culher.2013.07.006
- 1436 Pietruszczak, S. and Niu, X. (1992). A mathematical description of macroscopic behaviour of  
 1437 brick masonry. *International Journal of Solids and Structures*, 29(5), pp. 531-546. Doi:  
 1438 10.1016/0020-7683(92)90052-U
- 1439 Portioli, F., Casapulla, C., Gilbert, M. and Lucrezia, C. (2014). Limit analysis of 3D masonry  
 1440 block structures with non-associative frictional joints using cone programming. *Computers &*  
 1441 *Structures*, 143, pp. 108-121. Doi: 10.1016/j.compstruc.2014.07.010
- 1442 Psycharis, I.N., Fragiadakis, M. and Stefanou, I. (2013). Seismic reliability assessment of  
 1443 classical columns subjected to near-fault ground motions. *Earthquake Engineering &*  
 1444 *Structural Dynamics*, 42(14), pp. 2061-2079. Doi: 10.1002/eqe.2312
- 1445 Psycharis, I.N., Lemos, J.V., Papastamatiou, D.Y., Zambas, C. and Papantonopoulos, C. (2003).  
 1446 Numerical study of the seismic behaviour of a part of the Parthenon Pronaos. *Earthquake*  
 1447 *Engineering & Structural Dynamics*, 32(13), pp. 2063-2084. Doi: 10.1002/eqe.315
- 1448 Pulatsu, B., Erdogmus, E. and Bretas, E. (2018). Parametric study on masonry arches using 2d  
 1449 discrete-element modeling. *Journal of Architectural Engineering*, 24(2), p. 04018005 Doi:  
 1450 10.1061/(Asce)Ae.1943-5568.0000305
- 1451 Pulatsu, B., Erdogmus, E., Lourenco, P.B. and Quey, R. (2019). Simulation of uniaxial tensile  
 1452 behavior of quasi-brittle materials using softening contact models in DEM. *International*  
 1453 *Journal of Fracture*, 217(1-2), pp. 105-125. Doi: 10.1007/s10704-019-00373-x

- 1454 Pulatsu, B., Sarhosis, V., Bretas, E.M., Nikitas, N. and Lourenco, P.B. (2017). Non-linear static  
 1455 behaviour of ancient free-standing stone columns. *Proceedings of the Institution of Civil*  
 1456 *Engineers-Structures and Buildings*, 170(6), pp. 406-418. Doi: 10.1680/jstbu.16.00071
- 1457 Rafiee, A., Vinches, M. and Bohatier, C. (2008). Application of the NSCD method to analyse  
 1458 the dynamic behaviour of stone arched structures. *International Journal of Solids and*  
 1459 *Structures*, 45(25-26), pp. 6269-6283. Doi: 10.1016/j.ijsolstr.2008.07.034
- 1460 Remondino, F., Spera, M.G., Nocerino, E., Menna, F. and Nex, F. (2014). State of the art in  
 1461 high density image matching. *The Photogrammetric Record*, 29(146), pp. 144-166. Doi:  
 1462 10.1111/phor.12063
- 1463 Reyes, E., Gálvez, J.C., Casati, M.J., Cendón, D.A., Sancho, J.M. and Planas, J. (2009). An  
 1464 embedded cohesive crack model for finite element analysis of brickwork masonry fracture.  
 1465 *Engineering Fracture Mechanics*, 76(12), pp. 1930-1944. Doi:  
 1466 10.1016/j.engfracmech.2009.05.002
- 1467 Riveiro, B., Caamaño, J.C., Arias, P. and Sanz, E. (2011). Photogrammetric 3D modelling and  
 1468 mechanical analysis of masonry arches: An approach based on a discontinuous model of  
 1469 voussoirs. *Automation in Construction*, 20(4), pp. 380-388. Doi: 10.1016/j.autcon.2010.11.008
- 1470 Riveiro, B., Cabaleiro, M., Conde, B., Soilan, M. and Sanchez-Rodriguez, A. (2020). Laser  
 1471 scanning data for inverse problems in structural engineering, in: Riveiro, B. and Lindenbergh,  
 1472 R. (eds.) *Laser Scanning: An Emerging Technology in Structural Engineering*. pp. 215-225.
- 1473 Riveiro, B., Lourenço, P.B., Oliveira, D.V., González-Jorge, H. and Arias, P. (2016). Automatic  
 1474 morphologic analysis of quasi-periodic masonry walls from LiDAR. *Computer-Aided Civil and*  
 1475 *Infrastructure Engineering*, 31(4), pp. 305-319. Doi: 10.1111/mice.12145
- 1476 Roca, P., Cervera, M., Gariup, G. and Pelà, L. (2010). Structural analysis of masonry historical  
 1477 constructions. Classical and advanced approaches. *Archives of Computational Methods in*  
 1478 *Engineering*, 17, pp. 299-325. Doi: 10.1007/s11831-010-9046-1
- 1479 Rolin, R., Antaluca, E., Batoz, J.L., Lamarque, F. and Lejeune, M. (2019). From point cloud  
 1480 data to structural analysis through a geometrical hbim-oriented model. *Journal of*  
 1481 *Computational Cultural Heritage*, 12(2), pp. 1-26. Doi: 10.1145/3242901
- 1482 Sánchez-Aparicio, L., Villarino, A., García Gago, J.M. and González-Aguilera, D. (2016).  
 1483 Photogrammetric, geometrical, and numerical strategies to evaluate initial and current  
 1484 conditions in historical constructions: A test case in the church of san lorenzo (Zamora, Spain).  
 1485 *Remote Sensing*, 8(1), p. 60. Doi: 10.3390/rs8010060
- 1486 Sánchez-Aparicio, L.J., Riveiro, B., González-Aguilera, D. and Ramos, L.F. (2014). The  
 1487 combination of geomatic approaches and operational modal analysis to improve calibration of  
 1488 finite element models: A case of study in Saint Torcato Church (Guimarães, Portugal).  
 1489 *Construction and Building Materials*, 70, pp. 118-129. Doi:  
 1490 10.1016/j.conbuildmat.2014.07.106

- 1491 Sarhosis, V., Asteris, P., Wang, T., Hu, W. and Han, Y. (2016a). On the stability of colonnade  
1492 structural systems under static and dynamic loading conditions. *Bulletin of Earthquake*  
1493 *Engineering*, 14(4), pp. 1131-1152. Doi: 10.1007/s10518-016-9881-z
- 1494 Sarhosis, V., Asteris, P.G., Mohebkah, A., Xiao, J. and Wang, T. (2016b). Three dimensional  
1495 modelling of ancient colonnade structural systems subjected to harmonic and seismic loading.  
1496 *Structural Engineering and Mechanics*, 60(4), pp. 633-653. Doi: 10.12989/sem.2016.60.4.633
- 1497 Sarhosis, V., De Santis, S. and de Felice, G. (2016c). A review of experimental investigations  
1498 and assessment methods for masonry arch bridges. *Structure and Infrastructure Engineering*,  
1499 12(11), pp. 1439-1464. Doi: 10.1080/15732479.2015.1136655
- 1500 Sarhosis, V., Forgacs, T. and Lemos, J. (2020). Stochastic strength prediction of masonry  
1501 structures: a methodological approach or a way forward? *RILEM Technical Letters*, 4(0), pp.  
1502 122-129. Doi: 10.21809/rilemtechlett.2019.100
- 1503 Sarhosis, V., Forgács, T. and Lemos, J.V. (2019). Modelling backfill in masonry arch bridges:  
1504 A DEM approach. *9th International Conference on Arch Bridges*. Cham, Switzerland, 2-4  
1505 October 2019. Springer International Publishing, pp. 178-184
- 1506 Sarhosis, V. and Lemos, J.V. (2018). A detailed micro-modelling approach for the structural  
1507 analysis of masonry assemblages. *Computers & Structures*, 206, pp. 66-81. Doi:  
1508 10.1016/j.compstruc.2018.06.003
- 1509 Sarhosis, V. and Sheng, Y. (2014). Identification of material parameters for low bond strength  
1510 masonry. *Engineering Structures*, 60, pp. 100-110. Doi: 10.1016/j.engstruct.2013.12.013
- 1511 Selvaggi, I., Dellapasqua, M., Franci, F., Spangher, A., Visintini, D. and Bitelli, G. (2018). 3D  
1512 comparison towards a comprehensive analysis of a building in cultural heritage. *The*  
1513 *International Archives of the Photogrammetry, Remote Sensing and Spatial Information*  
1514 *Sciences*. Riva del Garda, Italy. Copernicus Publications, pp. 1061-1066
- 1515 Serpieri, R., Albarella, M. and Sacco, E. (2017). A 3D microstructured cohesive–frictional  
1516 interface model and its rational calibration for the analysis of masonry panels. *International*  
1517 *Journal of Solids and Structures*, 122-123, pp. 110-127. Doi: 10.1016/j.ijsolstr.2017.06.006
- 1518 Shen, Y., Lindenbergh, R. and Wang, J. (2016). Change analysis in structural laser scanning  
1519 point clouds: The baseline method. *Sensors*, 17(1), p. 26. Doi: 10.3390/s17010026
- 1520 Shen, Y.Q., Wang, J.G., Wei, S.F., Zheng, D.H. and Ferreira, V.G. (2019). Accurate extraction  
1521 of brick shapes in masonry walls from dense terrestrial laser scanning point cloud.  
1522 *Measurement*, 146, pp. 254-267. Doi: 10.1016/j.measurement.2019.05.086
- 1523 Shi, G.H. and Goodman, R.E. (1985). Two-dimensional discontinuous deformation analysis.  
1524 *International Journal for Numerical and Analytical Methods in Geomechanics*, 9(6), pp. 541-  
1525 556. Doi: 10.1002/nag.1610090604
- 1526 Shi, G.H. and Goodman, R.E. (1989). Generalization of two-dimensional discontinuous  
1527 deformation analysis for forward modeling. *International Journal for Numerical and*  
1528 *Analytical Methods in Geomechanics*, 13(4), pp. 359-380. Doi: 10.1002/nag.1610130403

- 1529 Simulia Inc. (2017) *Abaqus* ® *Version 6.17* [Computer program]. Available at:  
1530 <https://www.3ds.com/products-services/simulia/> [Accessed 19th January 2020]
- 1531 Sithole, G. (2008). Detection of bricks in a masonry wall. *The International Archives of the*  
1532 *Photogrammetry, Remote Sensing and Spatial Information Sciences. XXXVII*. Beijing. pp. 154-  
1533 165
- 1534 Šmilauer, V., Gladky, A., Kozicki, J., Modenese, C. and Stránský, J. (2010) *Yade, Using and*  
1535 *Programming. In Yade Documentation* [Computer program]. Available at: [http://yade-](http://yade-dem.org/doc)  
1536 [dem.org/doc](http://yade-dem.org/doc) [Accessed 19th January 2020]
- 1537 Smoljanovic, H., Nikolic, Z. and Zivaljic, N. (2015). A finite-discrete element model for dry  
1538 stone masonry structures strengthened with steel clamps and bolts. *Engineering Structures*, 90,  
1539 pp. 117-129. Doi: 10.1016/j.engstruct.2015.02.004
- 1540 Smoljanovic, H., Zivaljic, N. and Nikolic, Z. (2013a). A combined finite-discrete element  
1541 analysis of dry stone masonry structures. *Engineering Structures*, 52, pp. 89-100. Doi:  
1542 10.1016/j.engstruct.2013.02.010
- 1543 Smoljanovic, H., Zivaljic, N. and Nikolic, Z. (2013b). Overview of the methods for the  
1544 modelling of historical masonry structures. *Gradevinar*, 65(7), pp. 603-618. Doi:  
1545 10.14256/JCE.890.2013
- 1546 Smoljanovic, H., Zivaljic, N., Nikolic, Z. and Munjiza, A. (2018). Numerical analysis of 3D  
1547 dry-stone masonry structures by combined finite-discrete element method. *International*  
1548 *Journal of Solids and Structures*, 136, pp. 150-167. Doi: 10.1016/j.ijsolstr.2017.12.012
- 1549 Solla, M., Caamaño, J.C., Riveiro, B. and Arias, P. (2012). A novel methodology for the  
1550 structural assessment of stone arches based on geometric data by integration of  
1551 photogrammetry and ground-penetrating radar. *Engineering Structures*, 35, pp. 296-306. Doi:  
1552 10.1016/j.engstruct.2011.11.004
- 1553 Soni, A., Robson, S. and Gleeson, B. (2015). Structural monitoring for the rail industry using  
1554 conventional survey, laser scanning and photogrammetry. *Applied Geomatics*, 7(2), pp. 123-  
1555 138. Doi: 10.1007/s12518-015-0156-1
- 1556 Stavroulaki, M.E., Riveiro, B., Drosopoulos, G.A., Solla, M., Koutsianitis, P. and Stavroulakis,  
1557 G.E. (2016). Modelling and strength evaluation of masonry bridges using terrestrial  
1558 photogrammetry and finite elements. *Advances in Engineering Software*, 101, pp. 136-148.  
1559 Doi: 10.1016/j.advengsoft.2015.12.007
- 1560 Stefanou, I., Fragiadakis, M. and Psycharis, I. (2015). Seismic reliability assessment of classical  
1561 columns subjected to near source ground motions, in, pp. 61-82.
- 1562 Sutcliffe, D.J., Yu, H.S. and Page, A.W. (2001). Lower bound limit analysis of unreinforced  
1563 masonry shear walls. *Computers & Structures*, 79(14), pp. 1295-1312. Doi: 10.1016/S0045-  
1564 7949(01)00024-4

- 1565 Szakály, F., Hortobágyi, Z. and Bagi, K. (2016). Discrete element analysis of the shear  
 1566 resistance of planar walls with different bond patterns. *The Open Construction and Building*  
 1567 *Technology Journal*, 10, pp. 220-232. Doi: 10.2174/1874836801610010220
- 1568 Tang, P., Akinci, B. and Garrett, J. (2007) *Laser scanning for bridge inspection and*  
 1569 *management*. [Online]. Available at: [www.doi.org/10.2749/222137807796120283](http://www.doi.org/10.2749/222137807796120283) [Accessed  
 1570 19th January 2020]
- 1571 Tavafi, E., Mohebkhah, A. and Sarhosis, V. (2019). Seismic behavior of the cube of Zoroaster  
 1572 tower using the discrete element method. *International Journal of Architectural Heritage*, pp.  
 1573 1-17. Doi: 10.1080/15583058.2019.1650135
- 1574 Teza, G., Pesci, A. and Ninfo, A. (2016). Morphological analysis for architectural applications:  
 1575 Comparison between laser scanning and structure-from-motion photogrammetry. *Journal of*  
 1576 *Surveying Engineering*, 142(3), p. 04016004. Doi: 10.1061/(ASCE)SU.1943-5428.0000172
- 1577 Thavalingam, A., Bicanic, N., Robinson, J.I. and Ponniah, D.A. (2001). Computational  
 1578 framework for discontinuous modelling of masonry arch bridges. *Computers & Structures*,  
 1579 79(19), pp. 1821-1830. Doi: 10.1016/S0045-7949(01)00102-X
- 1580 TNO DIANA BV. Delft, N. (2020) *Diana ® Version 10.4* [Computer program]. Available at:  
 1581 <https://dianafea.com/diana-downloads> [Accessed 19th January 2020]
- 1582 Tobiasz, A., Markiewicz, J., Lapinski, S., Nickel, J., Kot, P. and Muradov, M. (2019). Review  
 1583 of methods for documentation, management, and sustainability of cultural heritage. Case study:  
 1584 museum of king Jan III's palace at Wilanów. *Sustainability (Switzerland)*, 11(24) Doi:  
 1585 10.3390/su11247046
- 1586 Truong-Hong, L. and Laefer, D.F. (2014). Octree-based, automatic building façade generation  
 1587 from LiDAR data. *Computer-Aided Design*, 53, pp. 46-61. Doi: 10.1016/j.cad.2014.03.001
- 1588 Tubaldi, E., Macorini, L. and Izzuddin, B.A. (2019). Identification of critical mechanical  
 1589 parameters for advanced analysis of masonry arch bridges. *Structure and Infrastructure*  
 1590 *Engineering*, pp. 328-345. Doi: 10.1080/15732479.2019.1655071
- 1591 Tucci, G. and Guardini, N. (2014). Rilevo e modellazione 3D a supporto dell'analisi strutturale:  
 1592 un approccio metodologico e sostenibile per il patrimonio architettonico (Italian). *Conference:*  
 1593 *Atti 18 Conferenza ASITA*. Florence, Italy. pp. 1197-1209
- 1594 United Nations (2016). *sustainable development goal 11*. Headquarters of the United Nations,  
 1595 New York, USA. [Online]. Available at: [https://www.local2030.org/library/60/SDG-Goal-11-](https://www.local2030.org/library/60/SDG-Goal-11-Monitoring-Framework-A-guide-to-assist-national-and-local-governments-to-monitor-and-report-on-SDG-goal-11-indicators.pdf)  
 1596 [Monitoring-Framework-A-guide-to-assist-national-and-local-governments-to-monitor-and-](https://www.local2030.org/library/60/SDG-Goal-11-Monitoring-Framework-A-guide-to-assist-national-and-local-governments-to-monitor-and-report-on-SDG-goal-11-indicators.pdf)  
 1597 [report-on-SDG-goal-11-indicators.pdf](https://www.local2030.org/library/60/SDG-Goal-11-Monitoring-Framework-A-guide-to-assist-national-and-local-governments-to-monitor-and-report-on-SDG-goal-11-indicators.pdf) [Accessed 19th January 2021]
- 1598 Valero, E., Bosche, F. and Forster, A. (2018). Automatic segmentation of 3D point clouds of  
 1599 rubble masonry walls, and its application to building surveying, repair and maintenance.  
 1600 *Automation in Construction*, 96, pp. 29-39. Doi: 10.1016/j.autcon.2018.08.018
- 1601 Vanin, F., Zaganelli, D., Penna, A. and Beyer, K. (2017). Estimates for the stiffness, strength  
 1602 and drift capacity of stone masonry walls based on 123 quasi-static cyclic tests reported in the

- 1603 literature. *Bulletin of Earthquake Engineering*, 15(12), pp. 5435-5479. Doi: 10.1007/s10518-  
1604 017-0188-5
- 1605 Vatan, M. and Arun, G. (2005). Using photogrammetric data for establishing 3D finite element  
1606 model of a masonry aqueduct. *CIPA 2005 XX International Symposium*. Torino, Italy, 26  
1607 September – 01 October, 2005. pp. 44-48
- 1608 Vincenzi, L., Bassoli, E., Ponsi, F., Castagnetti, C. and Mancini, F. (2019). Dynamic monitoring  
1609 and evaluation of bell ringing effects for the structural assessment of a masonry bell tower.  
1610 *Journal of Civil Structural Health Monitoring*, pp. 439–458. Doi: 10.1007/s13349-019-00344-  
1611 9
- 1612 Volk, R., Stengel, J. and Schultmann, F. (2014). Building information modeling (BIM) for  
1613 existing buildings — Literature review and future needs. *Automation in Construction*, 38, pp.  
1614 109-127. Doi: 10.1016/j.autcon.2013.10.023
- 1615 Vosselman, G. and Maas, H.-G. (2014) *Airborne and terrestrial laser scanning*. Illustrated,  
1616 reprint edn. Whittles Publishing.
- 1617 Westoby, M.J., Brasington, J., Glasser, N.F., Hambrey, M.J. and Reynolds, J.M. (2012).  
1618 'Structure-from-Motion' photogrammetry: A low-cost, effective tool for geoscience  
1619 applications. *Geomorphology*, 179, pp. 300-314. Doi: 10.1016/j.geomorph.2012.08.021
- 1620 Willis, A., Sui, Y., Galor, K. and Sanders, D. (2010). Estimating gothic facade architecture from  
1621 imagery. *IEEE Computer Society Conference on Computer Vision and Pattern Recognition -*  
1622 *Workshops*. San Francisco, CA, USA, 13-18 June 2010. pp. 43-48
- 1623 Wolf, P.R., Dewitt, B.A. and Wilkinson, B.E. (2014) *Elements of photogrammetry with*  
1624 *applications in GIS*. 4th edn. New York: McGraw-Hill Education.
- 1625 Yang, H. and Xu, X. (2019). Multi-sensor technology for B-spline modelling and deformation  
1626 analysis of composite structures. *Composite Structures*, 224 Doi:  
1627 10.1016/j.compstruct.2019.111000
- 1628 Ye, C., Acikgoz, S., Pendrigh, S., Riley, E. and DeJong, M.J. (2018). Mapping deformations  
1629 and inferring movements of masonry arch bridges using point cloud data. *Engineering*  
1630 *Structures*, 173, pp. 530-545. Doi: [10.1016/j.engstruct.2018.06.094](https://doi.org/10.1016/j.engstruct.2018.06.094)
- 1631 Zhang, S., Hofmann, M. and Beyer, K. (2018a). A 2D typology generator for historical masonry  
1632 elements. *Construction and Building Materials*, 184, pp. 440-453. Doi:  
1633 10.1016/j.conbuildmat.2018.06.085
- 1634 Zhang, Y. (2013) *Image-based geometric modeling and mesh generation*. 1st edn. Springer  
1635 Netherlands.
- 1636 Zhang, Y., Macorini, L. and Izzuddin, B. (2016). Mesoscale partitioned analysis of brick-  
1637 masonry arches. *Engineering Structures*, 124, pp. 142–166. Doi:  
1638 10.1016/j.engstruct.2016.05.046

- 1639 Zhang, Y., Macorini, L. and Izzuddin, B. (2017). Numerical investigation of arches in brick-  
1640 masonry bridges. *Structure and Infrastructure Engineering*, pp. 1-19. Doi:  
1641 10.1080/15732479.2017.1324883
- 1642 Zhang, Y., Tubaldi, E., Macorini, L. and Izzuddin, B. (2018b). Mesoscale partitioned modelling  
1643 of masonry bridges allowing for arch-backfill interaction. *Construction and Building*  
1644 *Materials*, 173, pp. 820-842. Doi: 10.1016/j.conbuildmat.2018.03.272
- 1645 Zucchini, A. and Lourenço, P.B. (2002). A micro-mechanical model for the homogenisation of  
1646 masonry. *International Journal of Solids and Structures*, 39(12), pp. 3233-3255. Doi:  
1647 10.1016/S0020-7683(02)00230-5

1648